

Single-molecule localization microscopy

Mickaë Lelek, Melina T Gyparaki, Gerti Beliu, Florian Schueder, Juliette Griffié, Suliana Manley, Ralf Jungmann, Markus Sauer, Melike Lakadamyali, Christophe Zimmer

▶ **To cite this version:**

Mickaë Lelek, Melina T Gyparaki, Gerti Beliu, Florian Schueder, Juliette Griffié, et al.. Single-molecule localization microscopy. Nature Reviews Methods Primers, 2021, 1 (1), pp.39. 10.1038/s43586-021-00038-x . pasteur-03695794

HAL Id: pasteur-03695794
https://pasteur.hal.science/pasteur-03695794

Submitted on 15 Jun 2022

HAL is a multi-disciplinary open access archive for the deposit and dissemination of scientific research documents, whether they are published or not. The documents may come from teaching and research institutions in France or abroad, or from public or private research centers.

L'archive ouverte pluridisciplinaire **HAL**, est destinée au dépôt et à la diffusion de documents scientifiques de niveau recherche, publiés ou non, émanant des établissements d'enseignement et de recherche français ou étrangers, des laboratoires publics ou privés.

Single-molecule localization microscopy

Mickaël Lelek[1], Melina T. Gyparaki[2], Gerti Beliu[3], Florian Schueder[4,5], Juliette Griffié[6], Suliana Manley[6]*, Ralf Jungmann[4,5]*, Markus Sauer[3]*, Melike Lakadamyali[7,8]*, Christophe Zimmer[1]*

[1]Imaging and Modeling Unit, Institut Pasteur, Paris, France
[2]Department of Biology, University of Pennsylvania, PA 19104-6058 USA
[3]Department of Biotechnology and Biophysics Biocenter, University of Würzburg, Am Hubland, 97074, Würzburg, Germany
[4]Faculty of Physics and Center for Nanoscience, Ludwig Maximilian University, Munich, Germany
[5]Max Planck Institute of Biochemistry, Matinsried, Germany
[6]Laboratory of Experimental Biophysics, Institute of Physics, École Polytechnique Fédérale de Lausanne (EPFL), Route Cantonale, Lausanne, Switzerland
[7]Department of Physiology, Perelman School of Medicine, University of Pennsylvania, Philadelphia, PA 19104-6058, USA
[8]Department of Cell and Developmental Biology, Perelman School of Medicine, University of Pennsylvania, Philadelphia, PA 19104-6058, USA

* corresponding authors

Author contributions: Introduction (M.Le. and C.Z.), Experimentation (G.B., F.S., J.G., S.M., R.J. and M.S.), Results (M.Le. and C.Z.), Applications (M.T.G. and M.La.), Reproducibility and data deposition (J.G., S.M. and C.Z.), Limitations and optimizations (M.T.G. M.La, F.S., R.J., M. Le and C.Z.), Outlook (M.T.G., M.La, G.B., F.S., R.J., M.S., M.Le. and C.Z.). Overview of the Primer (C.Z.).

Abstract

Single-molecule localization microscopy (SMLM) has emerged as a particularly powerful family of imaging techniques that dramatically improve the spatial resolution over standard, diffraction-limited microscopy techniques and can reveal biological structures at the molecular scale. In SMLM, individual fluorescent molecules are computationally localized from diffraction-limited image sequences, and the localizations are used to generate a super-resolution image, or in some cases a super-resolution movie or molecular trajectories. In this Primer, we first introduce the basic principles of SMLM techniques, then describe the main experimental strategies to perform SMLM, including fluorescent labeling, sample preparation, hardware requirements and image acquisition in fixed and live cells. We then explain how low-resolution image sequences are computationally processed to reconstruct super-resolution images and/or extract quantitative information, and highlight a selection of biological discoveries enabled by SMLM and closely related methods. We also discuss some of the main current limitations and potential artifacts of SMLM, as well as ways to alleviate them. Finally, we propose an outlook on advanced techniques and promising new developments in the fast-evolving field of SMLM. We hope that this Primer will be a useful reference for both newcomers and practitioners of SMLM.

[H1] Introduction

The spatial resolution of standard optical microscopy is limited to roughly half the wavelength of light[1], as a consequence of the optical phenomenon of diffraction. Because of diffraction, the 'point spread function' (PSF) — i.e., the image of an arbitrarily small source of light through a lens-based microscope — is not a point, but an Airy pattern, with a central peak approximately ~200-300 nm in width (**Fig. 1a**). Diffraction thus leads to a blurring of structures below this spatial scale. Although light microscopy has been used to study living organisms since the 17th century, the diffraction limit has severely restricted its ability to study subcellular organization at the scale of molecules or molecular complexes. For example, the structure of a nuclear pore complex, which is made up of hundreds of individual proteins, remains obscured by conventional light microscopy because the entire complex has a diameter of only ~120 nm (**Fig. 1b**). Over the past two decades, however, microscopy methods have emerged that overcome the diffraction limit and now enable insights into biological structures such as nuclear pores, viruses, chromatin complexes or cytoskeletal filaments closer to molecular scales[2]. The most well-known of these super-resolution microscopy methods fall into three main categories: stimulated emission depletion (STED)[3], structured illumination microscopy (SIM)[4,5], and single molecule localization microscopy (SMLM)[6-9] - the focus of this Primer. SMLM usually employs conventional widefield excitation, and unlike STED or SIM achieves super-resolution by localizing individual molecules[6-15]. Although each super-resolution method has its unique advantages and limitations and is optimally suited for different applications, as discussed elsewhere[2], SMLM has become broadly adopted in the life sciences owing to its high spatial resolution and relative ease of implementation.

SMLM is fundamentally based on the fact that the spatial coordinates of single fluorescent molecules (also called fluorophores, or emitters) can be computed with high precision if their PSFs are isolated (i.e. do not overlap). This is true because, with sufficient oversampling (magnification), subpixel shifts of the coordinates lead to predictable changes in pixel intensities (**Fig. 1c**). Localization precision can be defined by standard deviation of the scatter of localizations that would be obtained if a molecule was imaged and localized many times. For a single molecule, this precision is fundamentally limited by the number of photons relative to background and noise — the signal-to-noise ratio (SNR), with higher SNR allowing better precision — and not by the wavelength of light or the pixel size (**Fig. 1d**). In conventional widefield microscopy, nearby fluorescent molecules will have overlapping PSFs, preventing their localization (**Fig. 1b,f**). The central idea underlying SMLM is to avoid these overlaps by separating the fluorescent emissions of distinct molecules in time. The most common approach to obtain this temporal separation employs the fact that many fluorescent molecules can switch between an 'active' (or 'bright'/'ON') state, where they emit fluorescent light when excited, and one or more 'inactive' (or 'dark'/'OFF') states in which they do not (**Fig. 1e**). While this photo-switching of a particular molecule is a stochastic (i.e. random) event, the switching probabilities can be experimentally modulated – using specific fluorophores, laser irradiation, controlling the chemical environment or other means. Under suitable conditions, this allows one to ensure that at any given time only a small number of molecules are ON, and hence appear as spatially isolated, non-overlapping PSFs. Many thousands of image frames of the same field of view (FOV) are then typically acquired sequentially, so that many (ideally all) fluorescent molecules are ON in at least one frame of the sequence (**Fig. 1g**). The OFF/ON/OFF switching leads to a 'blinking' of the fluorophores in this

sequence of diffraction-limited images. These images are then processed computationally to detect all ON molecules (**Fig. 1h**) and determine their coordinates (**Fig. 1i**). Finally, all these localizations are accumulated to assemble a single image, whose resolution is no longer limited by optical diffraction (**Fig. 1j-l**). The resolution of this image is determined by the accuracy and precision with which individual molecules are localized, and by the distance between molecules whose coordinates contribute to the image, which itself depends on the density of molecules and the percentage of molecules that have been localized (**Box 1**).

While this general concept of sequentially imaging sparse random subsets of fluorophores and computing their positions is common to most forms of SMLM, there are multiple ways to perform SMLM, wherein technical choices will impact the spatial and temporal resolution, the ability to perform imaging in 2D or 3D, in one or multiple colors, in fixed or live cells and more. Instead of generating super-resolution images, very similar experimental approaches to SMLM can be used to track large numbers of single molecules in live cells in an approach known as 'single particle tracking PALM' (spt-PALM)[16].

A first key choice concerns the fluorophores and how they can be induced to switch between ON and OFF states. Fluorescence photoactivated localization microscopy[6,7,17] ((F)PALM) was initially demonstrated using fluorescent proteins (FP) that can be activated by UV illumination, while (direct) stochastic optical reconstruction microscopy ((d)STORM) and closely related methods[8,9,18] are based on synthetic fluorophores (dyes) that can photoswitch in the presence of suitable buffers. Point Accumulation In Nanoscale Topography[10] (PAINT) is a different SMLM approach that does not require photoswitching, but instead relies on fluorophores that switch between free diffusion and immobilization by binding to a target. The most prominent variant of PAINT is DNA-PAINT[19], where transient immobilization is achieved by hybridization of DNA strands.

A second key parameter is the labeling, i.e. how fluorophores are attached to the target molecule of interest, e.g. by genetic fusion with a FP or with antibodies.

A third important consideration for SMLM is how samples are prepared, e.g. whether and how they are chemically fixed and what buffer is used to enable or promote photoswitching.

Fourth, while the hardware requirements of most SMLM setups are relatively basic, the details of the optical system affect the resolution and ability to perform multicolor and 3D imaging.

A fifth choice is how image sequences are acquired, e.g. how many frames are taken and with what exposure time, and how laser power is set

Sixth, it is crucial to use appropriate software to computationally detect and localize (and possibly track) single molecules with high fidelity, and, if necessary to quantify the data.

Finally, SMLM can suffer from a number of artifacts such as sample drift or overlapping PSFs, that need to be addressed to ensure high quality images.

This Primer article aims to provide an introduction to all main facets of SMLM and some closely related approaches. The Experimentation section discusses experimental strategies including choice of fluorophores, labeling, sample preparation, optical system, and image acquisition. The Results section discusses how to computationally reconstruct and quantify SMLM images. The Application section highlights examples of biological applications made possible by SMLM. The remaining sections address issues of reproducibility and data deposition, explore limitations and

optimizations of current SMLM techniques, and finally provide an outlook on advanced and promising new approaches.

[H1] Experimentation

SMLM techniques critically require that the molecules to be imaged (typically, but not exclusively, proteins) be fluorescently labeled. In an ideal SMLM experiment, the function, location and number of target molecules would be preserved by the fluorescent labeling and each target molecule would be tagged at its exact position by exactly one fluorophore of minimal physical size (although some advanced studies label multiple sites of the same protein or DNA molecule to determine their 3D conformation, eg. [20,21]). To separate the fluorescent signals in time, each fluorophore would ideally be briefly active in one image frame and inactive otherwise, hence have high contrast ratio, and when active should emit a large number of photons relative to the background to enable high SNR and localization precision. For live cell super-resolution imaging, active fluorophores should also become inactive very quickly to enable rapid turnover and sampling, and imaging conditions should be compatible with maintaining the cellular physiology. Below, we discuss some of the main fluorophores and labeling approaches for SMLM relative to these ideal requirements. **Table 1** lists a selection of recommended ingredients for newcomers to SMLM.

[H2] Fluorophores for SMLM and how to switch them

SMLM fluorophores fall in one of five classes, depending on how they switch between ON and OFF states (**Fig. 2a-e**). Some of these classes include both synthetic dyes and FPs. Compared to FPs, synthetic dyes generally have higher photon counts and therefore better localization precision. FPs are generally more suited for live cell applications, but premature bleaching and/or incomplete labeling can further limit the structural resolution (**Box 1**). Note that for many fluorophores, the exact molecular mechanisms underlying photoswitching are still under investigation. We detail these five types of fluorophores and how to use them in SMLM below.

[H3] Photoswitchable fluorophores

Photoswitchable fluorophores (**Fig. 2a**) undergo reversible transitions from an ON to an OFF-state, such that a single fluorophore can blink many times. The first synthetic dyes used for SMLM were photoswitchable dyes, including carbocyanine dyes (Cy5, Alexa Fluor 647), rhodamine and oxazine dyes (e.g. most Alexa Fluor and ATTO dyes)[22]. These dyes can be reversibly switched between ON- and OFF-states upon irradiation with light of appropriate wavelength and using a photoswitching buffer consisting of PBS, 10-100 mM of a thiol such as mercaptoethylamine (MEA), and an enzymatic oxygen scavenger if necessary. Optimized buffers are available commercially (**Table 1**). Typically, UV light (λ_{ON}=405 nm) promotes activation from OFF to ON, while light of longer wavelength (e.g. λ_{OFF}=650 nm for Cy5) excites fluorescence and induces transition from ON to OFF. This photoswitching behaviour occurs either in the presence[23] or

absence of an activator dye[24] and laid the foundation for STORM[8] and *direct* STORM (*d*STORM)[9], respectively.

At the beginning of the experiment, all fluorophores reside in their ON-state. Hence, cells can be easily identified and brought into focus and, standard widefield images can be recorded for later comparison. To enable SMLM, the vast majority of fluorophores must then be turned OFF. This usually requires high irradiation intensities (~10-30 kW cm^{-2} at λ_{OFF}) over a few seconds. Once the density of active dyes is low enough to allow single molecule detection, the irradiation intensity can be decreased to ~1-3 kW cm^{-2}. This excitation pumps the active dyes to dark states (inactive triplet states), which are reduced by the thiol at pH > 7.0. The ON-state lifetime can be adjusted by the irradiation intensity, the thiol concentration, and the pH of the photoswitching buffer and is typically 5-20 ms, but can vary from 1 ms to 500 ms[25]. A recent study promotes the use of low excitation intensity and long exposure time to minimize initial photobleaching and improve resolution[26]. The reduced OFF-states exhibit a stability of several seconds before they are transferred back to the singlet ground state upon reaction with residual oxygen[27]. Direct excitation of the OFF-state at λ_{ON}=405 nm can be used to increase the activation and localization rate, e.g. for low density target molecules. While carbocyanine dyes perform better in the absence of oxygen, some oxazine dyes such as ATTO 655 also exhibit photoswitching in the presence of oxygen and require generally lower thiol concentrations. Therefore, it is recommended to vary the oxygen concentration to optimize the blinking performance for new dyes in (d)STORM experiments. Since cells contain the thiol glutathione at millimolar concentrations, some synthetic dyes can be used advantageously for live-cell *d*STORM[28]. For novices, we recommend to start with Alexa Fluor 647 or Cy5 in their first *d*STORM experiments (**Table 1**).

Photoswitchable fluorescent proteins (FPs) such as Dronpa[29] can be toggled reversibly from an OFF state to an ON state upon irradiation with different excitation wavelengths (λ_{ON}=405 nm, λ_{OFF}=488 nm) without requiring any special buffer. Moreover some “standard” FPs (e.g. YFP) can undergo a spontaneous recovery from OFF to ON states after partial photobleaching, but their use leads to localizing only a small subset of molecules, hence limiting resolution (**Box 1**).

[H3] Photoactivatable fluorophores

Photoactivatable fluorophores (**Fig. 2b**) essentially reside in their OFF state at the beginning of the experiment, i.e. the sample is dark, but these fluorophores can irreversibly switch to an ON state, either spontaneously or upon UV-light (λ=405 nm) activation under aqueous conditions. Synthetic photoactivatable dyes include photochromic rhodamine amides[30], the azetidinyl Janelia Farm (JF) rhodamine PA-JF$_{549}$ and silicon-rhodamine PA-JF$_{646}$[31], and the bridged carbocyanine Cy5B[32]. Because fluorophores are initially OFF, activation with 405 nm light is usually required to focus the microscope. To allow single molecule localization, photoactivated fluorophores must be photobleached, i.e. excited long enough until they permanently turn OFF, prior to activation of new fluorophores The PA-JF dyes exhibit usually longer ON-state lifetimes and deliver higher photon yields and localization precisions than the more common dyes they are derived from (e.g. ~5 nm) but, on the other hand, require longer total acquisitions times, typically exceeding several

hours. A benefit of these dyes is their membrane permeability, rendering them ideally suited for live-cell SMLM.

Photoactivatable fluorescent proteins include PA-mCherry, PA-mRFP (λ_{ON}=405 nm, λ_{exc}=564 nm), PA-mKate (λ_{ON}=405 nm, λ_{exc}=586 nm) and PA-GFP[33] (λ_{ON}=405 nm, λ_{exc}=488 nm) and have been used in the first demonstration of (F)PALM in fixed cells[6,7] as well as in live cells[16,34]. For most live-cell applications, photoactivatable FPs such as PAmCherry or PAtagRFP, are doubtless labels of choice. However, compared to most synthetic dyes, FPs have only moderate photostability and photon counts, reducing the localization precision[35] and requiring long acquisition times.

[H3] Photoconvertible fluorophores

Photoconvertible fluorescent proteins (**Fig. 2c**) including Eos[36] (and its derivatives like mEos2), Dendra2[36] and mMaple[37] can switch irreversibly from one spectral state (i.e. color) to another upon irradiation with light of appropriate wavelength. For example, Eos can be switched from green to red, by irradiation at $\lambda_{G\rightarrow R}$=405 nm, and is excited at λ_{G}=488 nm and λ_{R}=561 nm, respectively. For Dendra2, $\lambda_{G\rightarrow R}$=405 nm, λ_{G}=488 nm and λ_{R}=520 nm.

The signal of the (usually weaker) shorter wavelength fluorescence (before photoconversion) can be used to focus the sample and obtain a diffraction limited image before starting the SMLM image acquisition sequence. As for the photoactivatable fluorophores, after photoconversion, activated fluorophores must be photobleached to avoid PSF overlap with newly converted fluorophores, and the photobleaching time can be controlled by the irradiation intensity. Photoconvertible FPs are good choices for live cell SMLM.

[H3] Spontaneously-blinking dyes

Spontaneously blinking dyes (**Fig. 2d**) are based on a pH-dependent chemical reaction (intramolecular spirocyclization) and enable SMLM at defined pH in an aqueous solution[38] without requiring a photoswitching buffer. These dyes include the silicon-rhodamine dye HMSiR[39], HEtetTFER[40], and FRD[41]. These fluorophores exhibit excellent photon yield, are partially membrane permeable, and can thus be used advantageously in live-cell SMLM experiments. Spontaneously blinking fluorophores show immediate blinking from the onset of an SMLM experiment. The blinking kinetics is independent of the irradiation intensity and mainly controlled by the pH of the aqueous buffer. ON-state lifetimes vary in the range of 10-300 ms[38].

[H3] Temporarily binding dyes and DNA-PAINT

Unlike (F)PALM and (d)STORM, PAINT does not require fluorophores to switch between OFF and ON states. Instead, PAINT uses dyes[10] or dye-labeled ligands[42] that freely diffuse until they interact with targets of interest by either permanent or transient binding (**Fig. 2e**). Because free

dyes diffuse rapidly over many pixels during acquisition of a single image frame, they only appear as a blurred background and are not localized, whereas bound dyes appear as a PSF and are localized. This strategy effectively decouples the switching between ON and OFF-states from the dye photophysics. PAINT is not prone to photobleaching since the fluorophore reservoir can be replenished, and bright and photostable fluorescent dyes can be used. Any synthetic dye that exhibits a sufficient fluorescence quantum yield is compatible with PAINT.

DNA-PAINT[43] is a specific variation of PAINT that uses short (typically 6–10 nucleotide long) dye-labeled DNA oligonucleotides (called 'imager strands') that can transiently, yet sequence-specifically interact with their target-bound complements (called 'docking strands') (**Fig. 2e**). In DNA-PAINT, the ON-times (also called bright times, τ_b) can be almost arbitrarily tuned by the stability of the DNA duplex, as they are directly linked to the dissociation rate k_{OFF} of the imager-docking-duplex via $\tau_b = 1/k_{\mathrm{OFF}}$. Typical τ_b values are approximately 500 ms for an 8 bp duplex consisting of two CG and 6 AT pairs. As a rule of thumb, increasing the length by one bp results in roughly an order of magnitude increase in τ_b[43]. Fluorescence OFF-times (also called dark times, τ_d) are linked to DNA hybridization rates (k_{ON}) and imager concentration c_i via $\tau_d = 1/(c_i \cdot k_{\mathrm{ON}})$ and can be tuned by either changing c_i or k_{ON}. Bright times can be tuned to extract the highest number of photons per single binding event, resulting in high localization precisions down to ~1 nm[19,44].

[H2] Fluorescent labeling strategies

Several options are available to permanently or transiently link SMLM-compatible fluorophores to the molecules of interest. The main options are genetic fusion of a FP to the target protein; immunolabeling with synthetic dye conjugated antibodies; genetic fusion of the target protein with a tag that can bind to synthetic dyes; direct binding of synthetic dyes for specific structures and using labels for PAINT and DNA-PAINT. The choice of labeling strategy is critical, as it contributes to determining the resolution via the linkage error, i.e. the distance between the target molecule and the fluorophore (**Fig. 2f**), and via the labeling density. It also determines whether the target molecule retains its physiological localization and whether live cell imaging is possible.

[H3] Encoding fluorescent proteins

Genetically-encoded fluorescent proteins (FPs) are the most prominent labels for live cell fluorescence microscopy and have been used early on for (F)PALM in fixed[6] and live cells[16,45]. One labeling approach is to transfect cells using an expression vector containing DNA constructs consisting of the gene encoding the target protein genetically fused to the desired FP[46] (**Table 1**). An important disadvantage of transient transfection is that the number of expressed target proteins can vary widely. In stably transfected cell lines, the protein gene is overexpressed, to levels that can be controlled by construct optimization, but the endogeneous protein is left unlabelled. By contrast, CRISPR knock-ins allow for homozygous labeling of the endogenous genes, such that protein abundance is not altered and all target proteins are labeled. FPs exhibit a size of 2-5 nm and can thus also perturb protein functionality[47]. Nevertheless, in the ideal case

each protein of interest carries a single FP and shows wild-type functionality. For more details, see ref.[33,45,48,49].

[H3] Immunolabeling

Since synthetic dyes cannot be genetically encoded into biomolecules, they generally need to be coupled to other compounds, which can bind to a target molecule. Classical immunostaining, in which an antibody directed against an antigen enables binding of a specific biomolecule of interest, remains the standard method for labeling endogenous proteins in fixed cells. In direct immunolabeling, the antibody is chemically coupled to a synthetic dye (e.g. via NHS-chemistry), but indirect labeling using a second antibody that targets the primary antibody is often used to ensure higher and sensitivity and specificity (**Table 1**). Indeed, the binding of multiple secondary antibodies to a single primary antibody amplifies the fluorescent signal, and unlabeled primary antibodies can have better epitope binding affinity than primary antibodies modified for fluorescent labeling and hence less background. An important drawback of immunolabeling in SMLM, however, is that the commonly used immunoglobulin G antibodies are large (~10 nm), which entails a significant linkage error, especially with indirect labeling (linkage errors of ~20 nm). Camelid antibodies (nanobodies) are substantially smaller (~2.5-4 nm) and therefore offer an attractive alternative, especially for proteins tagged with GFP, for which highly specific nanobodies are available[50], or in combination with primary antibodies.

Since immunostaining of intracellular proteins requires permeabilization of cell membranes, it is also generally incompatible with live cell imaging, except for extracellular or membrane proteins, and in the latter case can modulate biological functions. The recent development of cell permeable nanobodies may however facilitate live cell immunolabeling in the future[51], as do electroporation based methods[52]. In general, it is important to check that the immunolabeling, permeabilization and fixation conditions allow specific labeling of the target proteins without artifacts[53].

[H3] Protein tags

To ensure specific labeling with minimal linkage error, an alternative are biorthogonal peptide-motifs or self-labeling protein tags including FlAsH tags, lipoic acid ligase, SNAP-tags, and Halo-tags[54-56]. These tags can be genetically co-expressed with a target protein and covalently bind their respective reagent or ligand, which is directly coupled to a fluorophore. These labeling methods combine genetic expression with the excellent photophysical properties of synthetic dyes, while reducing the linkage error to a few nanometers. Furthermore, they can be used for live-cell imaging experiments as long as the dye-substrate exhibits cell membrane permeability[57].

[H3] Direct labeling

Some biological structures can be labeled using dye conjugated small peptides or drugs, such as the bicyclic heptapeptide phalloidin or the taxane paclitaxel, which target actin and microtubule filaments, respectively[58,59]. However, despite their small size and minimal linkage error, such labels often impair biophysical function and act as biological modulators. Additionally, some

modified fluorophores can be directly integrated into the biostructure itself (e.g. organelle trackers or modified lipids)[60].

Regarding polypeptides or proteins, the smallest linkage error can be achieved via site-specific labeling of a single amino acid. Finally, genetic code expansion enables incorporation of custom-designed unnatural amino acids, such as TCO*-lysine, which can be directly coupled to functionalized synthetic dyes via fluorogenic click reactions without affecting biological functionality[61-63] and enabling live cell imaging.

[H3] PAINT and DNA-PAINT labeling

PAINT imaging has initially been restricted to imaging organelles for which transiently binding fluorescent molecules exist[10,42,64]. For example, PAINT was originally demonstrated by imaging large unicellular vesicles with the fluorophore Nile Red, which is only weakly fluorescent in water but becomes much brighter in a lipid environment[10] and has been applied to imaging DNA with dyes such as Hoechst[65]. DNA-PAINT, by contrast, can be used for any target molecule that can be linked to a docking strand. For this purpose, the most common approach is again immunolabeling, with unlabeled primary antibodies targeting the protein of interest and secondary antibodies conjugated to DNA docking strands using e.g. standard maleimide chemistry[19,66]. To overcome the large linkage errors of antibodies, DNA-PAINT has recently been combined with smaller and more efficient labeling reagents including nanobodies[66-68], genetically-encoded tags[67], affimers[69] and novel aptamer probes called SOMAmers[70].

[H2] Sample preparation

To achieve the sampling required for high resolution, dense structures such as the actin cytoskeleton generally require long acquisition times exceeding minutes. Therefore, cells and tissue samples must generally be fixed. Nevertheless, sparse and/or slowly moving cellular structures, such as focal adhesions[34] can to some extent be investigated using live cell SMLM. Below, we discuss sample preparation for fixed samples and live cell imaging.

[H3] Fixed samples

SMLM in fixed samples demands chemical fixation methods that crosslink proteins, preserve their binding sites and do not destroy molecular interactions. Aldehyde-based fixatives such as paraformaldehyde (PFA) and glutaraldehyde have been widely used in fluorescence imaging applications and are still among the most common fixation reagents for SMLM. Alternatives consisting of alcohols (e.g. ice-cold methanol) show efficient fixation especially for cytoskeletal components, but are unsuited to preserve the ultrastructure and molecular organization of cellular membranes or organelles. In addition, glyoxal has been suggested as an alternative fixative with improved preservation of cellular morphology for super-resolution microscopy[71]. For the investigation of dynamic biological processes or protein-protein interactions in membranes, residual mobility of membrane components must be considered, since it can induce artifacts such

as antibody cluster formation. To avoid residual mobility, membrane components should always be fixed using 4% PFA and 0.2% glutaraldehyde for 30 min or longer[72,73].

For immunolabeling, cells must also be permeabilized. After fixation and permeabilization, a blocking buffer such as bovine serum albumine (BSA) in PBS or normal goat serum (NGS) can be used to reduce non-specific binding and background signal before labeling[27]. In cryofixation, samples are very rapidly cooled down to cryogenic temperatures (<-150°C) under high pressure to prevent the formation of ice crystals. Although cryofixation is technically more demanding, has been mostly restricted to thin sections[6] and can affect photoswitching properties, it is compatible with both SMLM and electron microscopy and achieves optimal preservation of cellular ultrastructure[74,75] (see Outlook).

[H3] Live cells

For live cell experiments, after expression of the protein of interest and FP or labeling with tag substrates, cells are imaged in phenol red free medium or PBS. A major limitation of live cell SMLM are light-induced defects caused by high laser intensities (phototoxicity), especially at shorter wavelengths. A useful test for phototoxicity is to grow cells in medium overnight at 37°C and 5% CO_2 and check their survival using cell proliferation assays. A much more sensitive viability parameter is, however, if the irradiated cells undergo cell division during the next 20-24 hours after the SMLM experiment[76]. The illumination mode, irradiation wavelength and sample temperature should be adjusted to minimize phototoxic effects[76].

[H2] Optics of SMLM

Unlike other super-resolution methods, SMLM requires only a wide-field microscope equipped with standard continuous wave lasers for excitation and activation and a sensitive camera to detect single molecules (**Fig. 3a,b**). As a result of this relative simplicity, numerous commercial, low-cost open hardware, and homebuilt implementations exist[77-79]. SMLM compatible cameras are either electron-multiplying charge-coupled devices (EM-CCDs) or (back-illuminated) scientific complementary metal-oxide semiconductor (sCMOS) cameras. EM-CCDs use electron amplification gains that allow detection of single photons with negligible read-out noise and are particularly suited for low photon counts, despite multiplicative noise due to the stochastic amplification process. Modern sCMOS cameras have inhomogeneous read-out noise that requires extra correction, are somewhat less sensitive for weak signals, but have higher frame rates, larger chips (enabling larger FOV) and achieve similar SNR for bright dyes. The microscope body itself can be a standard commercial one, but many custom microscopes use more economical, minimal bodies and may lack an eyepiece and brightfield illumination (**Fig. 3b**). Because microscopes require much higher stability for SMLM than conventional microscopy, most commercial or custom microscopes include automated systems to keep the specimen in focus. For multicolor microscopy (see also **Box 2**), multiple laser lines can be combined and co-aligned using dichroic mirrors, which reflect and transmit only select wavelengths of light. Several

simple approaches are available to enable SMLM in 3D, e.g. through PSF engineering by inserting a cylindrical lens into the optical path[80] (**Fig. 3d,e, Box 4**). Widefield illumination of the sample can be generated by expanding a laser beam's circular intensity profile, then cropping the FOV to keep only the relatively uniform central area.

The sample's fluorescence emission is imaged through an objective lens onto the detector. Typically, a 60-100x, high numerical aperture (NA = 1.4 or higher) oil immersion objective is used to ensure efficient photon collection. When imaging samples close to the coverslip such as cellular membranes, total internal reflection fluorescent (TIRF)[81] or highly inclined and laminated optical sheet (HILO) illumination can be used to diminish out-of-focus background and thereby improve SNR and localization precision[82]. A dichroic is again used to separate excitation and emission light; for multicolor imaging a dichroic with multiple bandpasses can be chosen to reflect the excitation laser lines and pass emission wavelengths. For detection, the camera pixel size should be well-matched to the PSF size. The optimal magnification can be determined theoretically for specific background and photon numbers[83,84], but as a rule of thumb the pixel size should be approximately equal to half the PSF width. For example, for Alexa 647 dyes imaged with NA=1.4, the PSF width (FWHM) is 290 nm. With a 60x objective and an EM-CCD camera with 16 µm pixels, the pixel size in the sample plane is 267 nm, and hence too large, while with a 100x objective, the pixel size is diminished to 160 nm, allowing better localization precision.

[H2] Data acquisition in SMLM

In SMLM, the number of active fluorophores in each frame should be low enough to avoid PSF overlaps, but should be as high as possible to minimize acquisition time. However, experimentally optimizing active fluorophore density can be challenging; for photoswitching dyes, it results from a balance between excitation and activation laser intensities, and for PAINT from binding affinities and binder concentration. While these parameters are usually determined manually, SMLM can be automated with control software that implements a feedback loop to tune active fluorophore density[85-87].

[H3] Structural imaging in fixed cells

High-resolution studies of biological structures are generally done on fixed or purified samples, which allow for long acquisitions, to maximize the number of fluorophores localized and minimize motion artifacts.

The exposure time of each frame should ideally match the single molecule ON state lifetime, which is typically ~10-100 ms (see above). The total number of frames needed to reconstruct an image depends strongly on the structure being imaged and the desired resolution (**Box 1**). For higher-dimension structures (e.g. 2D membranes vs 1D filaments), the signal from an ON fluorophore will overlap with a larger portion of the structure and thus require more frames to reconstruct[88]. An accurate assessment requires a detailed analysis[34,88,89], but simple rules of

thumb give a rough estimate. For example, a structure like the centriole can be approximated as a hollow cylinder 250 nm in diameter and 400 nm long, for an area of $3x10^5$ nm^2, fitting into a single PSF. To resolve its surface at a scale of 20 nm would require that neighboring localizations should be at least that close to each other, but due to stochasticity and the need to oversample to build up the image, it ends up being at least 10 times as many, so approximately 5-10,000 molecules. With only one molecule 'ON' per frame, this implies that at least 10-20,000 frames should be collected. With a typical per-frame exposure time of 10-100 ms, this implies an acquisition time of 2-30 minutes.

[H3] Structural dynamics in live cell SMLM

For SMLM studies in live cells, two main imaging modes can be distinguished: structural dynamics and molecular dynamics (**Fig. 4**). Structural dynamics aims to reveal the time evolution of a structure composed of many molecules, such as a focal adhesion, a clathrin coated pit, or an organelle membrane[34,60,90]. In these studies, time series of super-resolution images are constructed from the localizations obtained in consecutive (non-overlapping) sets of frames (**Fig. 4a**). Choosing the number of frames in each set faces two conflicting requirements: more frames imply diminished temporal resolution and potentially motion blur, while less frames imply sparse sampling of the structure and hence worse spatial resolution[34] (**Box 1**).

[H3] Single molecule dynamics in live cells (spt-PALM)

The goal of molecular dynamics is to follow the trajectories of single molecules, often considering them as a probe of local environmental properties (**Fig. 4b**). Individual molecules are photo-converted, identified and tracked over multiple frames, in an approach first introduced as 'spt-PALM'[16]. In order to avoid misconnecting trajectories, the distance between molecules in each frame should be several times larger than the distance they travel between consecutive frames [16,42]. This implies that the density of active fluorophores must be significantly lower than for structural dynamics. Fluorophore motion between adjacent frames becomes a desired characteristic rather than a problem, so the time between frames should be chosen to allow molecules to move a distance greater than their localization precision. Although single molecule tracking existed before SMLM[91,92], the repeated photoactivation or photoconversion of fluorophores in live cells allows collection of orders of magnitude more molecular trajectories and hence enables much more detailed insights into molecular movements and the factors that control them[93].

[H1] Results

In SMLM, super-resolution images are not seen through the eyepiece of the microscope, but are assembled in a computer. Thus, the quality of super-resolution images strongly depends on image processing. Below, we discuss the computational aspects of SMLM data analysis. The majority of SMLM reconstruction methods can be decomposed in three main consecutive steps: single

molecule detection, single molecule localization, and super-resolution image rendering. We discuss these three steps in more detail below.

[H2] Single molecule detection

In the detection step, each diffraction-limited image is processed to determine the approximate location of active emitters. Before this, the image is often preprocessed to remove inhomogeneous background, e.g. using rolling ball, difference of Gaussians or wavelet filtering[94] or by estimating the background from the entire image sequence[95]. Detection is then typically done by extracting local maxima from the background-corrected image. Alternatively, the raw image can be searched for PSF-like patterns, e.g. by computing the correlation of this image with a small image representing the model PSF (e.g. a Gaussian approximation of the Airy function, or a more elaborate model for engineered PSFs in 3D SMLM, see **Box 4**) and thresholding the correlation image. The result is usually a set of pixel regions likely to contain single molecules. It can be shown mathematically that any detection algorithm will make false positives and/or false negatives, whenever images are corrupted by noise[96]. The lower the SNR of the image, the more unavoidable errors. Cameras used in SMLM can in principle have several sources of noise, including additive noise from thermal electrons (dark current noise), read-out noise, or multiplicative noise from stochastic amplification of photoelectrons. While read-out is usually negligible, dark noise can be reduced by using cooled cameras and multiplicative noise by setting low amplification gain, a fundamentally inevitable noise comes from the fact that fluorophores and the background emit only a finite number of photons, leading to Poisson noise. High photon counts relative to the background imply high SNR and therefore better detection performance.

[H2] Single molecule localization

In the crucial localization step, the pixel regions determined above are analyzed further to compute the subpixelic (x, y) coordinates of each molecule. We now briefly discuss the fundamental limits to localization precision and how localizations are computed.

[H3] Fundamental precision limits

Because of noise, localizations cannot be computed exactly, thus algorithms will make errors. These errors generally have random and systematic parts, as measured by the variance and the bias[83,84], and by precision and accuracy, respectively (see **Box 3**). Statistical estimation theory shows that the precision of an algorithm without bias is limited by the Cramer-Rao lower bound (CRLB)[97]. This limit depends on the SNR, with higher SNR allowing better precision. A well-known form of the CRLB is: $\sigma_{loc} \geq \sigma_0/\sqrt{N}$, where σ_{loc} is the precision, defined as the standard deviation of errors in estimating coordinates, σ_0 is the standard deviation of the PSF and N is the number of photons collected by the camera (see **Box 3**). Typical values are $\sigma_0 \approx$100 nm and $N = 10^2 - 10^4$, which would predict precision limits of $\sigma_{loc} \geq$1-10 nm. However, this simple formula is generally too optimistic, because it ignores factors such as non-Gaussian PSF shape, read and amplification noise, background signal, finite pixel size, and dipole orientation, all of which worsen

the precision limit. More complex expressions have been derived that take some or all of these factors into account[84,98], for example:

$$\sigma_{loc} \geq \sqrt{\left(\frac{\sigma_0^2 + a^2/12}{N}\right)\left(\frac{16}{9} + \frac{8\pi\sigma_0^2 b^2}{a^2 N^2}\right)}$$

where a is the pixel size, and b the background intensity[98]. The CRLB has become an essential notion in SMLM, because it defines a fundamental limit that all localization algorithms can (and should) be compared to.

[H3] Localization algorithms

Among the many different localization algorithms that have been proposed, the gold standard is maximum likelihood estimation (MLE), which approaches the CRLB for high SNR[84,98-100]. MLE aims to compute the (x, y) coordinates for which the probability $p(I; x, y)$ of obtaining the actually observed image I (the likelihood) is highest. To find this maximum, MLE algorithms employ an iterative procedure called 'gradient ascent', which starts from an initial position (x_0, y_0) (e.g. the center of a pixel identified in the detection step) and displaces it by small increments ($x_{n+1} = x_n + \delta x_n;\ y_{n+1} = y_n + \delta y_n$) designed to increase the likelihood, until it cannot be increased further. The same approach can be extended to compute 3D (x, y, z) coordinates (**Box 4**). In practice, MLE algorithms differ depending on the assumed mathematical model of image formation, including assumptions on PSF shape, background and noise, and MLE implementations may differ in technicalities of the gradient ascent procedure. On simulated images, MLE algorithms typically reach the CRLB, suggesting that their precision cannot be improved upon. A critical requirement to achieving this in practice is to have an accurate model of the PSF. The widely used Gaussian models are inaccurate, however, since they do not match the Airy patterns predicted from diffraction theory. More complex functions based on optical theory provide better PSF models, but may depend on unknown parameters and fail to capture aberrations due to imperfections of the optical system and/or induced by the sample. Therefore, it is preferable to calibrate PSF models, e.g. on real images of subdiffraction fluorescent beads by cubic spline fitting or phase retrieval, especially in 3D SMLMI[101,102]. Unsurprisingly, algorithms that use experimentally measured PSFs outperform those based on idealized PSFs[99]. Equally important is a good modeling (or subtraction) of the background, which is often assumed flat, but can also lead to biases in localizations if not properly accounted for. The iterative nature of MLE generally makes these algorithms slower than less precise non-iterative algorithms[79]. However thanks to GPUs and other optimizations, state-of-the-art MLE algorithms now typically allow real-time analysis of SMLM image sequences[99].

[H2] Postprocessing of localizations

After localizations are computed for all detected molecule, software apply post-processing steps to filter out suboptimal localizations, e.g. those with poor computed CRLB, or whose image does not match the model PSF well. Stringent filtering can easily improve the average localization precision, but will not necessarily improve resolution, because rejecting localizations compromises sampling (see **Box 1**). Another important post-processing step is to merge nearby

localizations in consecutive frames, which most likely arise from the same molecule, resulting in a single, more precise localization, without degrading sampling density. In addition, most SMLM experiments require drift correction, to be discussed later (see 'Limitations and optimizations').

[H2] Super-resolution image rendering

Once all diffraction-limited images have been processed, the extracted localizations are rendered in a new 'super-resolution' image. Typically, a grid is defined, with pixel sizes similar to the precision (say, σ_{loc}= 10 nm) and counting how many localizations fall into each bin (**Fig. 1k**). This 2D histogram is then visualized like any other image, with counts treated as intensities (**Fig. 1l**). Minor variations of this image rendering exist. For example, more weight can be given to localizations with higher intensities, or localizations can be replaced by Gaussian spots with a standard deviation given by their estimated precision (and normalized to an integral of 1 as probability densities). The resulting image should have sub-diffraction resolution, provided that certain conditions are met, as discussed in **Box 1**.

[H2] Software

Because computational processing is crucial to SMLM, over a hundred independent software packages have now been developed. To help users choose among this plethora of tools, a challenge has been organized that objectively compares many localization software on simulated images and a small set of experimental data, and its results are updated on a dedicated website[99,103]. Although these challenges are not without caveats (software are typically run by their authors and require expert fine-tuning, and results are contingent on the chosen simulation assumptions and experimental data), they provide a good starting point for state-of-the-art SMLM software. See **Table 2** for a selection of recommended software packages.

[H2] Quantitative analyses

Beyond generating super-resolution images for visual inspection, it is often desirable to extract quantitative information, such as the number, density or spatial distribution of molecules. The nature of SMLM data as molecular localizations opens distinct possibilities, but also comes with challenges. We discuss selected quantitative analyses methods for SMLM below.

[H3] Identifying clusters and counting molecules

One common question in SMLM studies of protein distributions is whether these form clusters, and if so of what size and stoichiometry. Analytic tools from spatial statistics such as Ripley's K function can help determine if a distribution of points in an image is clustered (or on the contrary exhibits spatial dispersion) and if so over which length scales. However, applying such tools to SMLM data is complicated by the fact that a single molecule often gives rise to a cluster of localizations owing to stochastic blinking and localization errors. Ignoring this can lead to artifactual clustering[104,105]. One approach to distinguishing apparent single molecule clusters from real molecular clusters is to determine the statistical distribution of localization errors, and apply pair-correlation analysis, as was demonstrated in an early study of membrane protein clusters[105].

This early method requires careful calibration, however, and although it provided average sizes of clusters, it cannot identify and measure individual ones. Analyzing clusters individually requires segmenting the image into groups of localizations. One proposed solution is a Bayesian method that can adapt to varying localization precisions[106], but requires strong assumptions on cluster shape. Alternative clustering methods include the density-based spatial clustering of applications with noise algorithm (DBSCAN) and tesselation-based approaches[107,108].

Once localizations are segmented into clusters, a common goal is to count the underlying target molecules. This is often challenging, however, because some target molecules may be localized many times, either because of repeated blinking (as in (d)STORM), or because they are labeled by multiple fluorophores (as in secondary immunolabeling), whereas others may not be localized at all for lack of labeling (as with partial transfection labeling) or failed photoactivation during acquisition time[104,105,109]. These confounding factors can be reduced, but not entirely eliminated, with endogenous homozygous labeling by pho toactivatable proteins. In general, calibration standards are a useful approach to account for repetitive blinking, but also failed photoactivation and variations in labeling stoichiometry[105,110-114]. Another approach to reduce counting errors is kinetic modeling of the photoswitching[115], which has been demonstrated successfully for photoactivatable proteins and shown to enable correct estimates of the number of copies of a molecular motor protein in bacteria[116]. However, modeling photoswitching kinetics in the presence of multiple dark states can be very complex. DNA-PAINT offers a particularly promising avenue for quantification thanks to well-known kinetics of binding. Its derivative qPAINT[117] uses the fact that binding frequency (assuming constant probe influx) scales linearly with the number of docking strands and thus targets. If calibrated for a single site, the number of targets in an unknown region can be calculated based on the observed blinking frequency, and the virtually unlimited sampling of target molecules allows minimization of statistical error.

[H3] Single particle reconstruction

For molecular complexes present in large numbers of identical copies, one can gain structural information at scales below SMLM resolution, by superimposing and averaging SMLM images of many individual structures after translations and rotations— as commonly done in electron microscopy[118,119]. The averaging allows measurement of structural features with a precision that is only limited by the number of imaged complexes, and not by single molecule localization precision. This approach has allowed determination of the radial position of nucleoporin epitopes within nuclear pore complexes with sub-nanometric precision[120] and has been extended to 3D applications to analyze the structure of human centrioles[119]. Single particle reconstruction is thus a powerful means to determine subunit architecture of large multi-protein complexes.

[H3] Colocalization analyses

Multicolor fluorescence microscopy is commonly used to determine if different molecules associate. In conventional microscopy, colocalization analyses typically measure the extent to which the diffraction limited signals from two or more channels overlap or correlate[121]. In multicolor

SMLM, strict colocalization should theoretically never occur, since distinct molecules cannot occupy the same physical location, and colocalization should be replaced by analyses of distances between molecules. Because of localization errors, however, individual localizations are better viewed as samples of probability densities, which can overlap for different color channels if molecules are closer than SMLM resolution. In principle, a simple way to assess colocalization is to apply established methods for conventional microscopy[121] to pairs of super-resolution images, but results can be strongly affected by stochastic blinking and/or background noise. Some recent methods therefore measure colocalization based on the localizations themselves, e.g. by adapting tools from spatial statistics or using tesselation-based segmentation of probability densities[122-124]. More work is needed to compare and improve colocalization methods against solid ground truth data. Regardless of the method used, chromatic aberrations can pose serious issues and must be carefully measured and corrected using, e.g. multicolor beads or fluorospheres.

[H3] Single molecule tracking

To quantify molecular dynamics in sptPALM[16], two main approaches can be distinguished: Lagrangian and Eulerian. Lagrangian methods focus on characterizing the dynamics of individual molecules by following them individually, for example by computing mean-squared displacements and estimating diffusion coefficients or transport states for each molecule[16,125] (**Fig. 4b**). Eulerian methods instead focus on individual regions in the sample and use the dynamics of molecules passing through them to infer local properties that characterize or affect molecule dynamics, e.g. maps of diffusivity or energy potentials[126]. For both approaches, it is important to take into account the fundamental uncertainties discussed above, to avoid biases in the analysis of molecular dynamics such as apparent subdiffusion or spurious energy potentials due to random localization errors[127,128]. More extensive discussions of single molecule tracking methods can be found in refs[93,129].

[H3] Other quantification methods

Many more methods have been developed to analyze SMLM point clouds in specific or generic contexts. These include various methods to segment structures from the background to analyze their morphologies, as shown e.g. for dendritic spines in neurons[108], or cytoskeletal filaments, e.g. to measure their orientation, lengths or curvature[130,131]. Another example are iterative hierarchical clustering methods, to classify the morphology of protein aggregates[132]. Given the variety of techniques and the current lack of comparative assessments, careful validation of each quantification method on simulated and experimental data remains critical. For more complete discussions of SMLM data analysis, see refs[107,133,134].

[H1] Applications

Compartmentalization of cells is crucial for regulating cell function. In recent years, SMLM has enabled us to visualize the spatial organization of proteins and nucleic acids within sub-cellular

compartments with nanoscale resolution. Below we summarize major new biology emerging from these studies, focusing on specific sub-cellular compartments including the nucleus, cell cytoplasm and plasma membrane.

[H2] Nucleus

Despite being a compartment of its own, the nucleus communicates with the rest of the cell through the nuclear pore complexes, transport portals that allow protein and nucleic acid exchange with the cytoplasm. Advances in SMLM have facilitated the study of the cell nucleus and the visualization of intranuclear structures and nuclear pores.

[H3] Chromatin Organization

Recent studies have demonstrated that chromatin is not randomly distributed inside the nucleus but is intricately folded and spatially organized[135]. SMLM methods are playing an important role in deciphering the organization of the human genome at length scales that are inaccessible to standard light microscopy (20-100 nm or 10 kB-1 Mb) and that are important for regulating gene function (for a recent review see ref[136]). Chromatin compaction has been thought to follow a hierarchical order where nucleosomes form a 10 nm fiber that resembles beads on a string, which further compacts into a 30nm fiber. However, this textbook view has been challenged in recent years. SMLM enabled the visualization of “nucleosome clutches” consisting of tens to hundreds of nucleosomes (few Kb in genomic scale and 20-100 nm in spatial scale) along the chromatin fiber in interphase nuclei of somatic cells. Similar results, in which nucleosomes pack into nanodomains of varying sizes were obtained by live cell super-resolution imaging[137] and recently recapitulated at specific genomic loci using mesoscale modeling[138]. While clutch size may be underestimated, especially in compact chromatin regions, due to imperfect labeling, these results suggest that chromatin packing in the nucleus is more heterogeneous than the regular 30 nm fiber (**Fig. 5a**)[139]. Clutch size was cell-type specific and depended on epigenetic histone modifications[140,141], suggesting that it can be a regulator of gene activity. While labeling of histones relies on immunostaining or over-expressing a tagged histone and the labeling efficiency depends on epitope accessibility to the antibody or the incorporation of tagged histones into nucleosomes, DNA itself can be labeled very efficiently using modified nucleotides and click chemistry[140,142]. Dual color SMLM imaging of histones and DNA showed a high level of co-localization between the two compartments as expected, suggesting that SMLM histone images are representative of chromatin organization within the nucleus[140].

Similarly, SMLM imaging of DNA labeled with Oligo-Paint probes showed that distinct epigenetic states follow distinct DNA packing and spatial organization in *Drosophila* cells[143]. In addition to the nucleosomal level, SMLM was also used to study larger chromatin domains including topologically associating domains (TADs), which are Megabase regions (100-500 nm length scale) of DNA determined by genome-wide chromosome conformation capture (Hi-C), within which DNA sequences interact more frequently with each other than with neighboring DNA sequences outside of TADs[144]. SMLM, in combination with multiplexed DNA-FISH (fluorescence in situ hybridization) methods, showed that the boundaries of TADs are more variable in single

cells than previously thought using population Hi-C[20,145], highlighting the importance of visualizing these small domains at high resolution in single cells.

For recent reviews of high resolution imaging of chromatin see refs.[136,146].

[H3] Transcriptional machinery and nuclear proteins

Live-cell SMLM has been used to visualize the dynamics and spatial organization of the transcriptional machinery, in particular RNA Polymerase II (RNA PolII)[147]. These studies showed that RNA PolII assembled into transient nuclear clusters, with lifetimes that correlated with their mRNA output, suggesting that they are transcriptionally active[148]. Follow up work showed that at least some of the RNA PolII clusters were phase separated liquid droplet condensates, particularly in genome regions known as super-enhancers[149]. SMLM further showed that several nuclear proteins, including architectural proteins like CCCTC-binding factor (CTCF) and the Polycomb group proteins, form nano-sized clusters within the nucleus[150,151]. Hence, clustering of nuclear proteins may be a general phenomenon for both shaping genome organization and regulating transcriptional output. Live cell SMLM will be important to determine if nuclear proteins form phase separated clusters that cannot be resolved with conventional microscopy.

[H3] Nuclear Pore Complex (NPC)

NPCs are excellent reference structure for characterizing and further improving super resolution microscopy modalities[113,152,153], and SMLM studies have helped to elucidate the structure of NPCs[120,152]. Most recently, live-cell high-speed single-molecule microscopy enabled the visualization of protein domains translocating through NPC channels and gave insight into transmembrane protein transport[154]. Finally, as previously mentioned, the arrangement of individual subunits within the NPC was elucidated by combining SMLM with single particle averaging[120,152] (**Fig. 5b**). This approach promises to be a powerful method for elucidating the subunit architecture of large multi-protein complexes.

[H2] Cytoplasmic contents

[H3] Microtubules

Microtubules were an early target structure to visualize with SMLM and validate SMLM methods due to their known shape and size (polymers with a diameter of 30 nm), as well as the abundance and ease of labeling of microtubule subunits (α-tubulin and β-tubulin)[80 155]. Besides being good test structures for SMLM, microtubules also play several important cellular functions including facilitating long-range transport and cell division. Combining super-resolution imaging of microtubules with single particle tracking of sub-cellular compartments enabled visualization of how these compartments are transported within the complex microtubule network in the crowded cell cytoplasm[156 157 158]. These studies uncovered that a special subset of microtubule tracks that are detyrosinated, play a crucial role in transporting and spatially organizing lysosomal and autophagosomal compartments to regulate autophagy[158].

[H3] Mitochondria, lysosomes and the endoplasmic reticulum

The photoswitching capability of common membrane probes specific to mitochondria, endoplasmic reticulum (ER) or lysosomes has further enabled visualizing the dynamics of these organelles with high spatial (30-60 nm) and temporal (1-2 s) resolution, revealing for example fusion and fission dynamics of individual mitochondria[60]. SMLM has resolved the organization of mitochondrial sub-compartments including mitochondrial inner and outer membrane, cristae and nucleoids[159]. SMLM revealed that mitochondrial nucleoids are heterogeneous in terms of their shape and size, are closely associated with the inner mitochondrial membrane, and that mitochondrial DNA inside nucleoids is more condensed than previously thought[160]. Low-resolution images suggested that the morphology of the ER consisted of tubules and sheets. Combining lattice light sheet (see 'Outlook') and PAINT, it was shown that these apparent ER-sheets are in fact very dense tubular structures, changing the textbook perception of this crucial organelle[161].

[H2] Plasma membrane

Because the plasma membrane can be imaged with TIRF[81], which affords improved resolution, SMLM is ideally suited to study the molecular organization of the plasma membrane with fluorescently labeled antibodies, toxins or ligands. SMLM has been instrumental in revealing that membrane receptors are often not uniformly distributed but sequester into small, functional nano-domains too small to be resolved with conventional light microscopy. One early PALM study showed for example how clusters of GPI-anchored proteins are disrupted by cholesterol depletion[105]. Recent studies used *d*STORM to investigate the effect of inflammatory activation on the clustering of tumor necrosis factor receptor 1 (TNFR1) [162] or the toll-like receptor TLR4[163], and sensitive detection of very low levels of an antigen in myeloma cells, with implications for cancer immunotherapy[164]. Earlier SMLM studies found that T cell antigen receptor (TCR) and linker for activation of T cells (Lat) are found in separate protein islands that concatenate after T-cell activation[165]. Subsequent studies revealed that TCR nano-clusters have a functional role in antigen recognition and therefore signal initiation[166]. However, this view has been recently challenged with quantitative super resolution imaging methods that attributed the clustering to overcounting artifacts[167], emphasizing the importance of careful quantitative analyses of SMLM data. More applications of SMLM to plasma membrane organization and associated challenges are discussed e.g. in ref. [168]

The plasma membrane interacts with the extracellular matrix (ECM) through focal adhesions, which are crucial both for cell adhesion and migration. iPALM, an advanced form of SMLM (see 'Outlook') was used to study the 3D organization of proteins within focal adhesions[169]. This work revealed the layered organization of focal adhesions, in which integrins and actin are separated by 40nm vertically (**Fig. 5d**), a region that comprises several layers; a membrane-apposed layer containing integrin tails, paxillin and focal adhesion kinase, an intermediate layer with talin and vinculin and an upper layer with actin regulators such as zyxin, α-actinin and vasodilator-simulated phosphoprotein. More recently, using SMLM, talin — but not vinculin — was identified as the primary determinant of focal adhesion organization as it diagonally spans the 40nm focal adhesion core region and acts as a molecular ruler[170].

[H2] Neuronal synapses and axons

Neurons are the most compartmentalized cells with a highly polarized and extended morphology in which the cell soma is separated from axonal, dendritic and synaptic compartments. The size of the synapse is below the diffraction limit, since the distance between the pre-synaptic and post-synaptic structures is ~20-30 nm. SMLM has been particularly useful in elucidating synaptic organization as it can readily resolve pre-synaptic and post-synaptic markers and determine the molecular architecture of proteins within synapses[171]. For example, SMLM revealed the nanoscopic organization of Bruchpilot (Brp) proteins within the synaptic active zone (AZ), a structure found within the presynaptic terminal in *Drosophila*[172]. Quantitative analysis further estimated the precise stoichiometry of the Brp proteins within nanoscopic complexes, showing that there are hundreds of these proteins within the AZ arranged in several heptameric clusters[172]. Moreover, SMLM allowed the detection of AMPA and NMDA receptor nanoclusters within the post-synapse, a finding with important implications for the regulation of synaptic transmission[173-175] and a recent *d*STORM study analyzed glutamate receptor clustering at presynaptic active zones of the mouse cerebellum[176].

Neuronal axons are densely packed with proteins, and therefore, challenging to image with conventional microscopy. One of the most striking findings enabled by SMLM was the discovery of actin rings with highly regular periodicity of <200 nm, wrapped around the circumference of neuronal axons (**Fig. 5c**)[58]. Moreover, spectrin also demonstrated similar periodicity to actin and was further shown to be interconnected with actin, resulting in the formation of a quasi-1D lattice structure, also known as the membrane-associated periodic scaffold (MPS).

[H2] Microbes

In addition to helping reveal the organization of cells, SMLM is well adapted to shed light on the inner structure of microbes and on how they can subvert the cellular machinery for their own purposes. SMLM is especially relevant for viruses, most of which are smaller than the diffraction limit, e.g. the HIV virion has a diameter of only ~100 nm. Unsurprisingly, SMLM or spt-PALM have been used to revisit the internal structure of all facets of their replication cycle from cellular entry, intracellular transport, replication, assembly, release and maturation for viruses such as HIV, herpes simplex virus, or respiratory syncitial virus[177-183] and SMLM approaches are also currently used to study SARS-CoV-2 infected cells. While bacteria are typically somewhat larger than the diffraction limit (~1 um in width and 2-3 um in length), SMLM has also proven very useful to analyze their internal architecture, for example to reveal the helical organization of the cytoskeletal protein FtsZ[184], or the organization of nucleoid associated proteins in *E coli*[185]. SMLM has also helped to clarify how bacteria interact with host cells, e.g. by visualizing septin cages entrapping Shigella as part of a cellular defense mechanism[186]. For more applications of super-resolution imaging to bacterial pathogens, see ref. [187].

[H1] Reproducibility and data deposition

SMLM involves a much larger number of experimental and analytical parameters than conventional microscopy studies. Furthermore, the intrinsic stochasticity of single molecule blinking makes typical SMLM images particularly noisy. These factors pose a challenge to

reproducibility of SMLM experiments. Therefore, it is especially important to carefully document experimental protocols and computational analyses and to make data and software available. On the software side, many free and open source software tools for SMLM are now available and have been compared using shared benchmarking data[99], but there is still a need to record and share the analysis parameters used, such as filtering on photon counts or localization precision. Competitions that benchmark downstream analyses such as cluster identification or single particle reconstruction will be useful to complement the challenges on localization. Platforms that integrate and compare existing tools would be useful to increase reproducibility of quantitative analyses.

On the data side, image deposition is increasingly recognized as important, leading to data sharing initiatives in the microscopy community, such as through archiving on Zenodo, FigShare, BioStudies and to some extent the Image Data Resource[188]. However, the large image volumes generated by SMLM experiments are an impediment to raw data sharing. Therefore, we propose that a good first step is to share localization data together with minimal information about the experiment. These data should include the target molecule(s) and/or epitope(s); the fluorescent labeling technique used with details of antibody concentrations and the functionality of FP tagging; the fixation protocol if relevant; microscope parameters such as laser wavelength, laser power density, camera type, exposure time, pixel size, objective magnification, numerical aperture and immersion medium; reconstruction software and parameters used, and a localization table including at least x,y coordinates and frame numbers, and preferably photon counts. A community resource that allows users to catalogue data doi with this information appended could catalyze data sharing and reuse and improve reproducibility in SMLM.

[H1] Limitations and optimizations

Although powerful, current SMLM techniques face a number of limitations. These include susceptibility to reconstruction artifacts, difficulties in imaging thick samples or tissues, and very low throughput, and limited applicability in live cell imaging. In this section, we highlight some of these limitations as well as optimizations to alleviate them.

[H2] Reconstruction artifacts and solutions

Several types of artifacts can affect the quality of reconstructed super-resolution images, including drift, overlapping PSFs, and localization biases.

[H3] Sample drift

A very common issue in SMLM is sample drift relative to the objective during image sequence acquisition, which is often unavoidable, even when using autofocus systems designed to limit axial drift . If ignored, even small drifts can result in blurring of the reconstructed image or even generate artefactual features, e.g. shadow microtubules[79] (**Fig. 6a**). However, drift can be measured, typically by tracking fiducial markers, such as fluorescent beads or gold coordinates

(which ideally remain fluorescent for the entire experiment), and the coordinates can then be corrected, simply by subtracting the estimated drift (**Fig. 6a, Table 1**). An interesting recent alternative is to estimate the drift from speckle patterns generated by back-scattered light[189]. For highly redundant structures such as microtubules, the lateral drift can also be estimated directly from the single molecule localizations alone using e.g. image cross-correlation, although this requires more caution[190,191]. Since axial drift can also deteriorate 2D SMLM images, 3D drift correction methods should be used whenever possible[102,189,192]. Many SMLM software packages provide drift correction tools (**Table 2**). Unlike drift, high frequency vibrations that affect localization precision by blurring individual diffraction-limited frames cannot be corrected computationally. Therefore, it is important to isolate the microscope from sources of vibration. The best way to avoid residual vibrations and drift artefacts is to eliminate them using active, real-time adjustment of the stage position[191,193,194]. For example, fiducial markers added to the coverslip can be tracked with a second camera and a closed loop system to drive piezoelectrical actuators that precisely reposition the stage[195]. Such approaches, although technically more demanding, can reduce drift to single nanometers or less[195-197].

[H3] Overlapping PSFs

Although the basic principle of SMLM assumes spatially isolated PSFs, avoiding PSF overlaps entirely is difficult, especially in high density regions. Furthermore, it can be desirable to increase the activation probability (hence leading to PSF overlaps) to increase imaging speed. Standard localization algorithms tend to treat overlapping PSFs as a single molecule and compute an incorrect position located somewhere in between. This can for example lead to an artificial blurring at intersecting filaments (**Fig. 6b**). In principle, such artifacts can be alleviated by stringent filtering of localizations for which the image deviates from that of a single PSF. However, stringent filtering can lead to reject most localizations and lead to the paradox that high density regions appear dimmer than low density regions in the reconstructed image (**Fig. 6c**). A simple but effective approach to detecting such artifacts is to verify if a blurred version of the super-resolution image is consistent with the widefield image. This approach yields a map that can highlight regions affected by reconstruction errors[198].

To avoid these artifacts and analyze images with high activation density, several 'multi-emitter fitting' algorithms have been developed that explicitly allow for PSF overlaps[99,103] or compute differences between consecutive images to create images closer to single molecule conditions[199]. Some related methods even dispense of the notion of localizing single molecules altogether[200]. These algorithms can indeed produce super-resolution images. However, overlapping PSFs necessarily imply significantly poorer resolution compared to low density SMLM regimes[99,103,201].

[H3] Other biases

Several other artifacts can occur in absence of drift or PSF overlaps. One example is a localization bias within the camera pixel, which can arise, for example, from ill convergence of MLE algorithms due to a mismatch between the model PSF and the actual PSF, and result in images with apparent grid patterns[202] (**Fig. 6d**). This type of bias can be easily identified from the histogram of localizations relative to pixel centers (**Fig. 6d**). It is less easy to identify spatially varying biases,

caused e.g. by a non-uniform background. One solution here is to take into account or eliminate non-uniform background by estimating it from individual images or from the entire image sequence[95]. Another common issue in 3D SMLM with engineered PSFs are aberrations due to refractive index mismatch between sample and oil, which can cause distortions along the axial dimension. Such distortions can be detected and prevented by careful calibration, typically by imaging fluorescent markers at known axial positions in the sample and adjusting the PSF model to fit them (**Box 4**)[102,203,204].

Another, much more fundamental and often overlooked localization bias stems from the fact that the PSF can depend on the orientation of the molecule's dipole, which is generally unknown. If the dipole remains fixed or constrained to certain angles during exposure time, ignoring dipole orientation can bias estimated positions by up to ~125 nm[205]. Recent work has shown that molecular positions and dipole orientations can be simultaneously estimated in advanced setups that feature polarizers and multiple cameras[206]. With standard SMLM systems, localization artifacts can fortunately still be avoided using fluorescent labels that rotate rapidly during the exposure time, such that all possible angles are equally sampled and biases are averaged out[206].

A very different type of artifact are unspecific detections that can arise from autofluorescence or impurities on the coverslip. Autofluorescence is stronger at shorter wavelengths, and can hence be alleviated using longer wavelength (redder) fluorophores and/or appropriate filters. Impurities can be reduced, though not entirely removed, by appropriate cleaning of coverslips, e.g. plasma cleaners[207] (**Table 3**).

[H2] Limitations for imaging tissues

Applying SMLM to tissues poses several challenges, some of which can be addressed by adapted sample preparation. A first challenge is fluorescent labeling. Tissues are thicker than cells and must be sufficiently permeabilized to be labelled properly. However, extensive permeabilization can compromise tissue structure. Additionally, fixed thick tissues are more likely to have background fluorescence and increased light scattering. One way to overcome the increased background/scattering problem is to cut tissues into thin slices and reconstruct a 3D SMLM image from many slices[208]. Cutting thin tissue slices often requires paraffin embedding of the tissue, which can make epitopes unavailable for antibody binding and can decrease labeling efficiency. Antibody labeling prior to embedding and using specific resins for the embedding step such as epoxy-resin can overcome this problem and also maintain high photon output of fluorophores[208]. Another solution to the fluorescent background problem is tissue-clearing[209 210], which together with other optimizations allowed to image high-resolution chromatin using *d*STORM in pathological tissue relevant for cancer diagnosis[210]. In this context, *d*STORM was also shown to be applicable to samples obtained by scalpel excision from tumor tissue[211]. Finally, SMLM puts additional demands on the way tissue samples are mounted, since sample drift must be avoided and specialized aqueous imaging buffers are required. To overcome this challenge, an imaging chamber was developed[209], consisting of a permeable agarose pad and a custom-built stainless steel imaging adapter to keep tissue slices flat, immobile and bathed in imaging buffer during image acquisition.

Optical systems adapted to imaging thick samples and tissue without slicing will be discussed in the 'Outlook' section.

[H2] Throughput limitations

A major limitation of SMLM techniques is their limited throughput, i.e. the low number of cells imaged per unit time, which results from a relatively small FOV, and the fact that it typically takes minutes or more to obtain a high quality super-resolution image of a single animal cell. This severely restricts the ability of SMLM to image large areas or tissue volumes or to reveal rare cellular phenotypes. Furthermore, SMLM approaches are typically limited to a few colors because of the small number of spectrally distinguishable fluorophores. Nevertheless, several efforts have been deployed to address these limitations:

[H3] Larger fields of view

Initial SMLM studies were often restricted to a FOV of, say ~25x25 µm, because they relied on EMCCD cameras with 512x512 pixel arrays, and because non-uniform laser illumination typically results in spatially varying photoswitching and photon emission rates, therefore requiring cropping of images to the central region of this array, where illumination is approximately constant. Much larger FOV can now be obtained using sCMOS cameras with bigger arrays (2024x2024 pixels) and methods to homogenize illumination (flat-fielding)[212-214]. For example, a low-cost microlens array (MLA)-based epi-illumination system -flat illumination for field-independent imaging (FIFI) increased the FOV to 100x100 µm[213], hence allowing to image ~2-5 mammalian cells simultaneously with high resolution.

[H3] Multiplexing

Several multiplexing approaches have been developed to image more than a few molecular species in the same sample[215,216]. DNA-PAINT is particularly amenable to multiplexing because DNA sequences provide exquisite programmability and specificity. In Exchange-PAINT[216], different molecular targets are simultaneously labeled with orthogonal DNA docking strands, followed by sequential delivery, imaging, and washing steps using complementary imager strands (**Fig. 6e,f**). Importantly, each imager species can carry the same dye, since target identity is encoded by the respective sequence and imaging round as opposed to the dye color[217]. Similar approaches can also be used with sequential labeling of proteins by different primary antibodies, using the same dye-conjugated secondary antibodies. For example, maS^{3}TORM (multiplexed automated serial staining stochastic optical reconstruction microscopy) enabled SMLM of 15 target proteins in single cells[215].

To increase throughput in multiplexed DNA-PAINT, target molecules can furthermore be engineered to blink with precisely adjustable frequency and duration, thereby providing a distinct "kinetic barcode" for the simultaneous detection of hundreds of unique molecular species[218]. In a related approach, frequency multiplexing DNA-PAINT modulates the excitation lasers at different frequencies and uses Fourier transformation to unmix the fluorescent response, hence enabling simultaneous imaging of several fluorophores[219].

Note that highly multiplexed approaches such as MERFISH or seqFISH+ are now increasingly used to visualize thousands of distinct RNA species or DNA-loci in single cells. Although they rely on sequential labeling rather than photoswitching, these methods enable super-resolution views into 3D genome structure and cellular transcriptome. For more information, see refs.[146,220].

[H3] Automation

To perform high throughput or multiplexed imaging for more than a few conditions or target proteins, one needs a fully automated microscope solution that allows fluid exchange, can perform staining, sample positioning and image acquisition. The automation problem is being addressed through several recent developments. Combining high-content screening concepts with SMLM through an automated microscope and automated data analysis, (HCS)–SMLM enabled 3D imaging of an entire 96-well plate[221]. The fluid exchange problem was tackled using a fluidics system composed of low cost Lego hardware controlled by ImageJ software[222]. The above-mentioned maS^{3}TORM used a fully automated and coordinated 3D SMLM microscope with a pipetting robot to perform staining experiments in situ[215]. An example biological application of automated SMLM image acquisition and analysis (though not with automated staining) is the study of 23 proteins involved in yeast endocytosis[87].

[H3] Faster SMLM

Increasing FOV improves throughput, but not the speed and temporal resolution of SMLM, which typically remain poor. Nevertheless, tremendous progress in optimizing the speed of SMLM has been made since the first PALM study, which required ~2-12 h for a single FOV. Using sCMOS cameras with high (>1 kHz) frame rates and synthetic dyes, the rate of localization can be dramatically increased, although this requires high laser powers (>50 kW cm^{-2}) to maintain good SNR and localization precision[25,223]. Such optimizations allowed for example 2-color 3D SMLM of more than 10,000 mammalian cells in ~26 hours[224].

DNA-PAINT has traditionally been a particularly slow SMLM technique. The influx rate of dye-labeled imagers to their targets, which ultimately determines the achievable acquisition speed, is limited by the overall DNA association rate k_{on} (~ 10^6 (Ms)$^{-1}$), leading to a blinking event every 100 s for typical imager concentrations of 10 nM) and the imager concentration. While increasing the imager concentration can in principle speed-up DNA-PAINT, concentrations in excess of a few tens of nM would increase background fluorescence, hence reduce SNR and reduce precision. To address this, FRET-based approaches have been implemented[225-227], effectively suppressing fluorescence from diffusing imager strands. Orthogonal approaches aim at increasing k_{on}. This can be done by rational sequence design and buffer optimizations, leading to an order of magnitude faster k_{on} and thus imaging speed[228]. Another approach to increase k_{on} is based on preloading DNA-PAINT imager strands with Argonaute proteins[229]. The latest development is the use of periodic, concatenated sequence motifs of rationally designed sequences, which now speeds up DNA-PAINT by 100-fold over the classical implementation[230].

[H3] Cheaper SMLM

Although the cost of SMLM hardware, especially custom-built setups, is moderate compared to other advanced microscopy systems, typical systems still have price tags on the order of ~100,000 € or more. However, efforts to replace expensive components by cheaper alternatives (e.g. EMCCDs by sCMOS cameras or scientific grade lasers by LEDs) and/or leverage smartphone technology have resulted in prototypes ~10 k€ or less[77,231-233]. Although they do not always achieve the spatial resolutions of more sophisticated microscopes, such approaches may prove sufficient for many applications and could also enable large-scale parallelization and hence gains in throughput.

[H2] Structural dynamics limitations

Perhaps the most severe limitation of standard SMLM is its restricted applicability to study structural dynamics in live cells. Live-cell structural studies are rare, because collecting enough localizations to provide a super-resolution snapshot of a biological structure before it rearranges is generally challenging it not impossible. While the above speed optimizations with high frame rates are applicable to fixed cells, the intense laser excitation required for fast turnover is much more problematic for live cells because of its adverse effects on cell physiology (phototoxicity), especially when using UV activation[34], and rapid photobleaching. Because of these constraints, structural SMLM studies have for the most part been limited to technical proofs of principle or to relatively slowly moving structures with few reconstructed snapshots[34,85,90,223]. As discussed above, methods designed for higher activation densities can overcome this limitation to some extent, but at the cost of a significant reduction in spatial resolution.

[H1] Outlook

We conclude this Primer with a look at advanced SMLM techniques and particularly promising ongoing developments that aim to address some of the main remaining challenges in SMLM. These include: imaging the ultrastructural context, moving towards truly molecular resolution, imaging thick samples and tissues, imaging live samples without phototoxicity or photobleaching and more.

[H3] SMLM with light sheets

To overcome the challenges of imaging deep inside thick tissue, SMLM was combined with light sheet fluorescence microscopy (LSFM) for imaging live[234] and fixed tissues[89]. In LSFM, the sample is illuminated with a thin light sheet perpendicular to the optical axis[235]. This optical sectioning is advantageous for living tissues, as they experience much reduced irradiation and hence less stress during imaging, but also for fixed tissues, as background fluorescence is significantly reduced and contrast is improved. In individual molecule localization-selective plane illumination microscopy (IML-SPIM), a cylindrical lens is used to create activation and readout light sheets to photoactivate single fluorescent molecules in thick tissue[234]. More recently, lattice light sheet (LLS) microscopy was combined with 3D *d*STORM for plasma membrane receptor

imaging on the basal and apical membrane as well as for 3D single-particle tracking[236] and tissue imaging by PAINT using newly developed membrane probes[89], achieving multi-color super resolution imaging of samples up to 20 μm thick and whole-cell 3D SMLM of intracellular membranes. The contrast achieved with this approach resembles that achieved with heavy metal-stained EM images, without mechanical sectioning. Light sheet SMLM can further be combined with Adaptive Optics (AO) to correct for PSF aberrations induced by the scattering tissue to improve the imaging depth and spatial resolution when imaging thick samples[237].

[H2] Combining electron microscopy and SMLM

Electron microscopy (EM) generally offers even better spatial resolution than SMLM, and also provides a global view of the cellular ultrastructure that SMLM does not. Conversely, EM lacks the molecular specificity afforded by fluorescence. Super-resolution visualization of specific molecules within an ultrastructural context is possible by combining EM with SMLM on the same sample (Correlative light and electron microscopy; CLEM). For example, combining platinum replica electron microscopy (PREM) (a technique where the sample is coated by a heavy metal to increase its contrast by EM), with iPALM and STORM, provided important details about the distinct structural zones inside clathrin-coated structures[238,239]. Similarly, SMLM and PREM allowed to show that actin rings found in neurons consist of long, intertwined actin filaments, revealing an unexpected braid-like organization of actin rings[240]. Correlative cryogenic SMLM (cryo-SMLM) and electron tomography was demonstrated to study the subcellular localization of important regulatory proteins in *Caulbacter crescentus*[241]. In a recent tour de force, fluorescently labeled high-pressure frozen cells were preserved in vitreous ice, imaged with cryo-SMLM and subsequently with 3D focused ion beam scanning electron microscopy (FIB-SEM), and the images resulting from the two modalities were registered to nanoscale precision. This approach achieved ~40nm resolution visualization of protein distribution within frozen whole cells in 3D in the context of their ultrastructure[242] and revealed unexpected relationships between different cellular compartments, such as the existence of ER proteins inside the nucleus. These methods, while requiring challenging sample preservation and preparation, nonetheless hold great promise for visualizing various molecular complexes in their ultrastructural context.

[H2] SMLM with opposing objectives

Because localization precision critically depends on the SNR, one way to improve resolution is to collect more photons from single fluorophores. This can be done using two opposing objectives (4 Pi setups) that collect twice as many photons from single fluorophores as single objective systems, thus improving localization precision by a factor $\sim\sqrt{2}$. Such systems enabled lateral resolutions <10nm and, in combination with astigmatism (**Box 4**) axial resolution <20nm in 3D STORM, allowing to distinguish individual actin filaments and to visualize two distinct layers of actin networks that showed sheet-like protrusions[243]. Interferometric PALM (iPALM) [244] also uses two opposing objectives, but allows laser beams to interfere in a three-way beam splitter and propagate to 3 CCD cameras, allowing to determine the 3 coordinates of fluorescent molecules. In contrast to PSF shaping or multi-plane systems (see **Box 4**), iPALM does not trade off localization precision for axial range and achieved isotropic <20 nm 3D resolution with fluorescent

proteins. More recently, interferometric SMLM has been extended to achieve 10-20 nm resolution imaging of the ER, mitochondria, NPCs, bacteriophages and other structures in whole mammalian cells without compromising resolution[245]. Careful calibration of refractive index variations will be needed to extend this approach to whole nuclei.

[H2] SMLM with minimum fluxes

Since the onset of SMLM, the dominant paradigm to increase localization precision has been to collect more photons from single fluorophores, as in the methods above. This paradigm has meanwhile been shifted by the introduction of MINFLUX[246], a concept for localizing single emitters not by their highest intensity, but by lowest emission fluxes arising from a local minimum in excitation. In the original implementation, an excitation doughnut in combination with a three-point-estimator was used to precisely determine the emitter position (**Fig. 7a**). In combination with photoswitching, MINFLUX attains single nanometer resolution with considerably reduced photon counts compared to standard SMLM (**Fig. 7b**). This allows for very high localization precisions, even with relatively dim FPs, and >100-fold faster single molecule tracking than previous methods[246].

Recently, two independent groups have replaced the excitation doughnut by a standing wave to spatially modulate excitation intensities, either using diffraction gratings (SIMFLUX[247]) or optical interference (Repetitive Optical Selective Exposure or ROSE[248]). In both implementations, localization precision is improved by ~2-fold compared to standard SMLM. While MINFLUX can theoretically achieve arbitrarily high localization precision, SIMFLUX and ROSE possess the advantage that image acquisition times do not scale with FOV, thus currently offer faster acquisition speed.

With further advancements (e.g. 3D, multicolor, live cell imaging)[249] and simplification to hardware and software, these methods are poised to set a new standard for molecular-resolution SMLM.

[H2] SMLM in expanded samples

Whereas almost all super-resolution methods aim to diminish the size of the effective PSF[2], expansion microscopy (ExM) takes an entirely orthogonal approach and improves resolution by physically expanding a sample embedded in a polyelectrolyte hydrogel[250] (**Fig. 7c**). Although ExM can achieve super-resolution with conventional microscopes (e.g. 70 nm resolution with five-fold expansion[250] or 25 nm with 20-fold expansion[251]), combining it with SMLM can potentially improve resolution down to single nanometers. An important challenge is that many of the targeted molecules can lose their label after free-radical polymerization of the hydrogel, compromising labeling density and resolution[252]. Furthermore, addition of photoswitching buffer as required for *d*STORM leads to shrinking of polyelectrolyte hydrogels. Finally, expansion of prelabelled samples results in further displacement of the fluorophore from the target molecule, increasing the linkage error, e.g. from 17.5 nm with indirect immunostaining to 70 nm after 4-fold expansion, again severely limiting the resolution. Recently, trifunctional linkers have been developed that are inert to polymerization, digestion and denaturation, and enable direct labeling and covalent linking of target molecules and functional groups to the hydrogel[253,254]. Furthermore,

it was shown that re-embedding of the expanded hydrogel prevents shrinking and post-expansion labeling preserves the ultrastructure of multiprotein complexes, improves the labeling efficiency and reduces the linkage error from 17.5 nm to ~5 nm for 3.2-fold expansion[255]. The potential of these new methods has been demonstrated by imaging of clathrin-coated pits, microtubules and centrioles with ~5 nm resolution[255 254] (**Fig. 7d**). Ex-SMLM thus provides another promising road map for achieving true molecular resolution.

[H2] Enhanced SMLM with deep learning

The increasingly complex imaging data acquired thanks to advances in SMLM exacerbate the demand for computational analysis. In recent years, the field of computer vision has been revolutionized by machine learning methods based on multi-layer artificial neural networks (deep learning)[256]. Unsurprisingly, deep learning is now also adapted to advance light microscopy methods, including SMLM[257]. For example, deep learning has been used to extract single molecule localizations from diffraction-limited images, including in high activation density conditions, which can dramatically reduce processing time compared to MLE[258]. However, deep learning can also help accelerate image acquisition itself by overcoming apparently fundamental sampling constraints. This is possible because deep learning can reconstruct high quality images from much fewer localizations than traditionally needed[259] by learning structural redundancies from similar images (**Fig. 7e**). With further adaptations, such methods might greatly facilitate super-resolution in live cells while minimizing phototoxicity, as recently demonstrated for 3D light sheet microscopy[260]. Deep learning will certainly also make inroads in the quantitative analysis of SMLM data, such as the segmentation of biological features [261,262].

The power of deep neural networks comes from their ability to learn complex features from training data. However this reliance on training data also carries the risk that neural network outputs might be biased towards the training data, potentially leading to miss novel phenotypes or even to generate artifacts[257,259,263]. This well-known Achilles heel of machine learning therefore calls for careful validations and/or retraining of existing deep learning frameworks and the development of methods that are aware of or robust to mismatches between testing and training data. If these challenges are correctly addressed, machine learning methods will likely play a key role in overcoming key limitations of advanced microscopy and SMLM in particular.

[H2] Concluding remarks

SMLM is a powerful, yet relatively accessible, family of imaging technique that combines fluorophore chemistry, optics and computation to image and analyze biological structures and/or dynamics at increasingly higher resolution. In this Primer, we attempted to introduce all main basic aspects of SMLM, highlighting biological applications that illustrate the maturity of SMLM methods, while also covering advanced and promising recent developments. As the SMLM field continues to evolve, it brings us nearer to a future where all molecules within a cell, tissue or organism may be individually localized, counted and tracked. We hope that this Primer will encourage more investigators to adopt and further improve SMLM to explore the innermost architecture and mechanisms of living systems.

1186
1187
1188

TABLES

Table 1: Selected commercial reagents for SMLM experiments

This table lists examples of some recommended reagents for newcomers to SMLM. For multi-color imaging, see **Box 2**. For more comprehensive information and/or systematic comparisons of SMLM labeling techniques, see e.g. [35,36,60,264,265] and the protocols listed in **Table 3**.

Type of reagent	Reagent(s)	Supplier	Reference	Application
Primary antibodies, unlabeled (use with labeled secondary antibodies)	Rat anti-tubulin antibody (recognizes the α subunit of tubulin)	Bio-Rad	link	(*d*)STORM of microtubules
	Rabbit anti-nucleoporin Nup133	Abcam	link	(*d*)STORM of nuclear pores in human cells
Secondary antibodies conjugated to synthetic dyes (use with unlabeled primary antibodies)	Anti-rat antibody coupled to Alexa Fluor 647	ThermoFisher	link	*d*STORM
	Anti-rabbit antibody coupled to Alexa Fluor 647	Jackson ImmunoResearch	link	*d*STORM
Fluorescent protein plasmids	mEos3.2 plasmid	Addgene	link	(F)PALM
	mMaple3 plasmid	Addgene	link	(F)PALM
DNA-PAINT kits	DNA-conjugated secondary antibodies/nanobodies (docking strands)	Massive Photonics	link	DNA-PAINT
	Dye-conjugated DNA (imager strands)	Massive Photonics	link	DNA-PAINT
Direct labeling	Phalloidin conjugated to Alex Fluor 647	ThermoFisher	link	*d*STORM of actin
	MitoTracker Red	ThermoFisher	link	Live cell STORM of mitochondrial membranes
Photoswitching buffers	SAFe Reagents	Abbelight	link	(*d*)STORM
	Everspark	idylle	link	(*d*)STORM
Labeled samples	Cells with labeled microtubules, mitochondria, podosomes..	Abbelight	link	(*d*)STORM
Fiducial markers	TetraSpeck microspheres (100 nm diameter)	ThermoFisher	link	Correction of drift and/or chromatic aberrations

Table 2: Selected SMLM software

This table lists a few recommended software packages for SMLM image reconstruction. All listed software are free, can reconstruct 3D SMLM images and all except SMAP enable drift correction. This selection is partly subjective, as it is based on software known to (and in part developed by the authors), but also based on objective results from the 2D/3D SMLM localization challenges. For more details and quantitative comparisons of these and many other SMLM software (currently 95), we refer to the challenges and their updates (http://bigwww.epfl.ch/smlm).

Software name	URL	Comments	Reference
ThunderSTORM	https://zitmen.github.io/thunderstorm/	Widely used, implements multiple 2D and 3D algorithms. Strong performance in 2D SMLM challenge	94
SMAP	https://github.com/jries/SMAP	Handles arbitrary PSFs; Strong performance in 3D SMLM challenge	266,267
SMOlphot	https://bitbucket.org/ardiloot/smolphot-software/wiki/Home	Strong performance in 3D SMLM challenge	NA
ZOLA-3D	https://github.com/imodpasteur/ZOLA-3D	Handles arbitrary PSFs and refractive index mismatch	102
Picasso	https://github.com/jungmannlab/picasso	Software package optimized for DNA-PAINT	19

Table 3: Selected experimental protocols for SMLM

The following is a non exhaustive list of some recommended experimental protocols for SMLM.

- Van de Linde et al. (ref. [27]) : *d*STORM, live cells.
- Gould et al. (ref. [202]) : (F)PALM.
- Schnitzbauer et al. (ref. [19]): DNA-PAINT, multicolor, quantification (qPAINT).
- Jimenez et al. (ref. [268]): *d*STORM, DNA-PAINT, multicolor, optimized sample preparation.
- Manley et al. (ref. [269]): spt-PALM.
- Kaplan et al. (ref. [270]): sample preparation optimized for *d*STORM in yeast.
- Davis et al. (ref.[207]): how to prepare coverslips to minimize impurities in SMLM

FIGURE LEGENDS

Figure 1: Principle of SMLM.
a) A single fluorescent molecule (green dot) imaged through a microscope appears on the camera as a fuzzy, ~200 nm wide spot (the PSF) extending over multiple pixels. **b**) PSFs from simultaneously emitting molecules overlap if their distances are smaller than the PSF. **c**) The (X_0,Y_0) coordinates of a single molecule can be computed with high precision, because subpixel displacements (e.g. here by 0.5 pixels in X and Y) lead to predictable changes in pixel values, as shown by the grey scale image (bottom) and corresponding 2D histogram (center) (simulated data). The mesh surface shows a Gaussian model PSF centered on (X_0,Y_0). **d**) Higher photon counts (N) lead to higher SNR images and more precise localizations (red crosses). **e**) SMLM usually exploits the fact that fluorophores stochastically switch between an active ('ON') state and one or more inactive ('OFF') states. **f**) A diffraction-limited image of nuclear pores, with all fluorophores ON, is blurred by overlapping PSFs. **g**) A sequence of diffraction-limited images of the same area, where only few molecules are ON simultaneously. **h,i**) In each frame, single molecules are computationally detected (**h**) and localized (**i**). Molecules at the border of the image are not detected. **j**) An SMLM experiment results in a localization table, where each row represents a distinct localization event and columns indicate x, y coordinates and additional information, e.g. frame number and photon counts (N). There are usually multiple localizations per frame, and the same molecule can be localized in multiple frames. **k,l**) Accumulated localizations visualized as a scatter plot (**k**), or a 2D histogram (**l**), with bins much smaller than raw image pixels. The raw image pixels are shown by the dashed grid, and 10x10 small bins are shown inside a single raw image pixel in **k**). This 'super-resolution' image reveals the ring-like (octagonal) structure of nuclear pores that was previously hidden.

Figure 2: Fluorophore types and labeling strategies in SMLM.
a-e) Fluorophores compatible with SMLM can be divided into five classes: photoswitchable (**a**), photoactivatable (**b**), photoconvertible (**c**), spontaneously blinking (**d**), or temporarily binding (**e**). The boxes indicate properties of fluorophores in each class and an example fluorophore. The schematic involving the lambda symbol indicates the nature of switching that enables SMLM. **f**) Comparison of different fluorescent labeling approaches and the resulting linkage error, i.e. the distance between the molecular target of interest (here, tubulin) and the fluorophore. From left to right: immunolabeling with primary and secondary antibodies (orange); labeling with a small camelid antibody (nanobody, yellow), often in combination with primary antibodies or GFP (green); labeling with a genetically encoded protein such as Eos (magenta) or a self-labeling protein tag; direct labeling with a dye-conjugated ligand such as the microtubule-binding compound docetaxel (turquoise box); incorporation of unnatural amino acids such as TCO*-lysine (blue box) via genetic code expansion (GCE) enables rapid labeling with functionalized synthetic dyes. Structure of immunoglobulin (PDB-ID 1IGT), green fluorescent protein bound to enhancer nanobody (PDB-ID 3K1K), EOS-FP (mEos2, PDB-ID 3S05), exemplified target protein (tubulin, PDB-ID 1FFX).

Figure 3: SMLM Hardware.

a,b) A basic SMLM setup consists of illumination (laser, Köhler lens, i); imaging optics and stage (objective, sample, ii) and detection (tube lens, camera, iii). Dichroic mirrors are used to separate excitation and emission wavelengths, and can be combined with additional emission filters to reject autofluorescence. **c**) A 2D *d*STORM image of microtubules. **d**) A 3D SMLM system can be obtained simply by adding an optical component to engineer the PSF, such as a cylindrical lens, which generates astigmatism. **e**) A z-stack of a fluorescent bead shows the axial variations of an astigmatic PSF. **f**) A 3D super-resolution image obtained by analysis of 2D single molecule images, displayed here in 2D with color indicating z. Here, PSF calibration and image reconstruction was performed with ZOLA-3D[102].

Figure 4: Live cell SMLM

a) Structural dynamics of a focal adhesion (tdEos-paxillin) reveal its appearance near the cell edge before maturation and motion toward the interior. Each super-resolution image is reconstructed from 1,000 raw frames. Scale bar: 500 nm. From ref. [34]. **b**) Molecular dynamics of the vesicular stomatitis virus glycoprotein (VSVG-tdEos), a transmembrane protein freely diffusing on the plasma membrane. The motion of each protein is traced over multiple frames, with different colors representing individual molecules (left). Each trajectory can be analysed, to create a map of diffusion coefficients (center). In contrast, the dynamics of molecules within the actin cytoskeleton (actin-tdEos) show directed motion near the cell's leading edge and diffusive motion toward the interior (right). Scale bars: 500 nm. From ref. [16].

Figure 5. Major discoveries enabled by SMLM

a) STORM image of histone H2B in human fibroblast cells (hFb) with progressively higher zoomed insets, adapted from ref.[139]. Scale bars: 2 um and 500 nm. **b**) Top: *d*STORM image of nuclear pore complexes (NPCs) labeled with antibodies against the nucleoporin Nup133. Three individual NPCs are shown on the right and an average image of 4,171 aligned NPCs on the lower right. Scale bars: 0.5 um and 0.1 um. Bottom: Left: Colored circles show radial positions of different nucleoporins in the plane of the nuclear envelope, determined from averaged images, with the inferred position of the Y-shaped scaffold complex overlaid. Circle thickness reflects 95% confidence intervals of average radial distances. Center and right: side and frontal views of the EM structure (grey), with the radial positions of nucleoporins shown in color, and two positions of the Y complex consistent with the data overlaid. Scale bar, 40 nm. From ref.[120]. **c**) iPALM image of a human U2OS cell expressing integrin α_v-tdEos (left) and actin-mEos2 (right) with color coded zoomed insets of boxed regions adapted from[169]. Colors represent the z-position relative to the substrate (z=0 nm). Scale bars: 500 nm. **d**) 3D STORM image of actin in a neuronal axon with zoomed y/z insets of boxed regions showing actin rings, adapted from[58]. Scale bars: 1 um and 200 nm.

Figure 6: Limitations and optimizations

a) SMLM image of microtubules before and after drift correction. Arrows show a fluorescent bead used to estimate the drift. **b,c**) Artifacts due to PSF overlaps in simulated images. **b**) Left: ground truth image without localization errors, shown as a scatter plot. Middle: SMLM image for a low density of activated fluorophores (10 localizations per μm^2, no PSF overlaps). Right: the same, for a high activation density (50 localizations per μm^2); overlapping PSFs cause artifactual

localizations near the center. **c**) Simulated molecular clusters, with a 10-fold higher density for the top cluster. Left: simulated ground truth shown as scatter plot. Middle: SMLM image without filtering. Right: the same after filtering of poor localizations due to overlapping PSFs. After filtering, the high density cluster is barely visible. **d)** Artifacts in SMLM images of microtubules resulting from subpixel localization bias. Top: without bias. Bottom: with bias; the bias is due to computational localization with an incorrect PSF model. As a result of bias, the reconstructed image shows a grid pattern. Insets show the entire FoV. The localization bias is readily apparent in the histogram of x coordinates relative to the center of pixels in the raw images (drift correction was not applied to better highlight the effect of localization bias). **e**) Exchange-PAINT implements sequential imaging of multiple targets by DNA-PAINT with different imager strands labeled with the same dye. The sample is first labeled with orthogonal docking strands P_1, P_2,.., P_n, then the first imager strand species P^*_1 , complementary to docking strand P_1 , is introduced and a DNA-PAINT image of P_1 is acquired. Next, the strands P^*_1 are washed out, then imager strands P^*_2 are introduced and a DNA-PAINT image of P_2 is acquired, etc. for *n* cycles. Each DNA-PAINT image is assigned a distinct pseudocolor and all *n* images are then superposed. **f**) Pseudocolor DNA-PAINT images of origami structures displaying digits 0–9. Scale bar: 25 nm.

Figure 7: New directions in SMLM

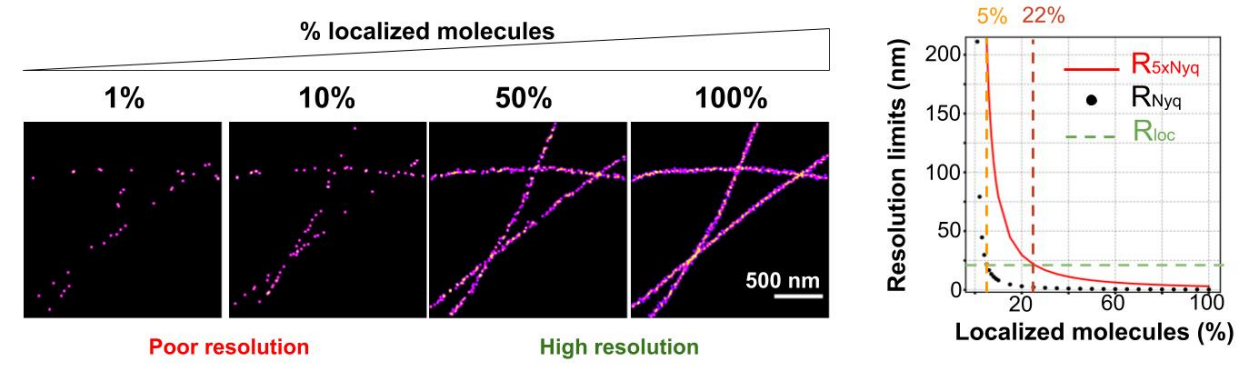
a,b) MINFLUX. **a**) MINFLUX excitation concept to precisely probe emitter positions by minimal photon fluxes. A doughnut-shaped excitation (green) is moved sequentially to four probing positions r_0, r_1, r_2, r_3 (colored circles) in the vicinity of a single fluorophore (orange star). The probing range is given by L. If the doughnut center coincided perfectly with the fluorophore position, no photons would be emitted. The position of the fluorophore can be calculated with very high precision from the fluorescence photon counts shown below. From ref.[246]. **b**) Example nuclear pore complex imaged by MINFLUX. Scale bars: 50 nm. From ref. [249] **c,d**) Expansion-SMLM. **c**) In expansion microscopy (ExM), samples are embedded in a gel that expands upon hydration. Immunolabeling of epitopes can be performed before or after gelation and expansion using linkers that bind to the gel and to a fluorophore. Full or partial protein digestion is commonly used to enable isotropic expansion. In order to enable (*d*)STORM imaging in photoswitching buffer the sample is re-embedded in an uncharged polyacrylamide gel after expansion. **d**) Left: 3D post-labeling Ex-dSTORM image of a 3.2x expanded and re-embedded sample shows the ninefold symmetry of the procentriole. Scale bar, 500 nm. Right: 3.1-fold expanded and re-embedded tubulin filaments. Magnified view of highlighted region (white box). xz side view cross section of a tubulin filament showing its hollow structure. Scale bars, 2 µm (large square), 500 nm (vertical rectangle), 200 nm (small square). From ref.[255] **e**) Deep learning accelerates SMLM image acquisition. A widefield image (WF) and a sparse SMLM image obtained from k=300 frames only are fed as inputs to an artificial neural network (ANN) that was previously trained on high quality (long acquisition) SMLM images of microtubules. The ANN outputs a super-resolution image that is in good agreement with an SMLM image obtained from k=30,000 frames ('ground truth'), suggesting a 100-fold reduction in acquisition time without compromising spatial resolution. Adapted from ref[259].

BOXES

Box 1: The resolution of SMLM images

Determining the resolution of an SMLM image is not straightforward. The resolution R cannot be better than $R_{\mathrm{loc}} \approx 2.3\ \sigma_{\mathrm{loc}}$, thus estimating localization precision σ_{loc} is key. One approach to estimate σ_{loc} is to calculate the Cramer-Rao lower bound (CRLB), but this estimate is generally too optimistic. More realistic estimates can be obtained from the standard deviations of coordinates in small localization clusters likely originating from single molecules. However, both estimates ignore potential localization biases or linkage errors. A common alternative is to calculate the dispersion of coordinates (e.g. the full width half maximum, or FWHM) across thin structures such as cytoskeletal filaments. This provides a conservative upper limit to $2.3\ \sigma_{\mathrm{loc}}$, since the FWHM reflects both precision and the width of the labeled structure (including linkage errors).

A critical, but often overlooked requirement to achieving a resolution $R_{\mathrm{loc}} = 2.3\ \sigma_{\mathrm{loc}}$ is to have a good sampling, i.e. a sufficiently high percentage of localized molecules. An early study introduced a Nyquist sampling criterion to calculate the sampling limit (R_{Nyq}) to resolution based on the nearest neighbor distances between localizations[34], but a reanalysis suggested that 5-fold higher sampling ($R_{5\mathrm{xNyq}}$) is actually required[89]. In the simulated images below, with $\sigma_{\mathrm{loc}} = 10\ \mathrm{nm}$, this criterion implies that 22% of molecules must be localized to achieve a resolution $R_{\mathrm{loc}} = 23$ nm. A Fourier Ring Correlation (FRC) criterion[271] — which measures the correlation between subsets of localizations — simultaneously accounts for localization precision and sampling, but requires a user-defined threshold and can hide spatial variations in resolution. More recently, an alternative, threshold-free approach based on phase correlation was proposed[272].



While useful, such measures are insufficient to rigorously determine the resolution. Compelling evidence that an image has resolution R or better is to clearly distinguish distinct structures at distances $\leq R$. In biological samples, this is done most convincingly on complexes where molecules are located at known distances from each other, such as nuclear pores, which have therefore become a gold standard to evaluate resolution[113].

BOX 2: Multicolor SMLM

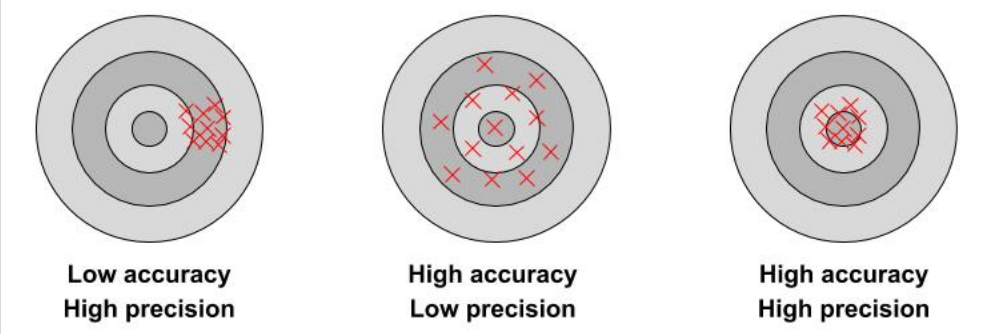
The investigation of biomolecular interactions in cells requires super-resolution imaging of multiple target molecules in one experiment. Multicolor SMLM with synthetic dyes can be accomplished using the classical STORM concept with probes that contain both an activator and a reporter fluorophore[8]. Here, various activator-reporter dye pairs attached to an antibody, such as Alexa Fluor 405 & Cy5, Cy2 & Cy5, and Cy3 & Cy5, enable multicolor STORM using three different activation lasers and spectrally-selective activation of the reporter fluorophore Cy5[273].

Activator-free SMLM with synthetic dyes (*d*STORM) requires fluorophores that exhibit similar blinking efficiency under identical photoswitching buffer conditions. Suitable pairs for two-color *d*STORM include Alexa Fluor 532 & Alexa Fluor 647, ATTO 520 & Alexa Fluor 647, and CF 568 & Alexa Fluor 647, as well as combinations with longer-wavelength absorbing dyes, e.g. DyLight 750[152,274].

To avoid chromatic aberrations, multicolor SMLM by spectral-demixing can be used. Here, one can use synthetic dyes that exhibit good photoswitching performance in the same thiol switching buffer and can be efficiently excited with the same laser wavelength but exhibit different emission maxima. The emission light is spectrally separated by a dichroic beamsplitter and imaged onto two cameras or separate parts of the same camera chip. The fluorophores are then classified by their emission ratio. Alternatively, the emission signal of different synthetic dyes can be split into two detection paths and recorded simultaneously on two cameras (or two regions of the same camera): one emission spectra recording and one for localization[275-277]. FPs have also been used successfully for multicolor SMLM, either alone, e.g. Dronpa & mEos, or in combination with synthetic fluorophores, e.g. mEos2 & Alexa Fluor 647 or Dronpa & Alexa Fluor 647[177,278].

Box 3: Localization precision, accuracy and the Cramer-Rao lower bound

The image I of a single fluorophore is the result of a stochastic process that depends on several unknown parameters, notably the (x, y) coordinates of the molecule and the number of collected photons, N. Localization algorithms attempt to determine (x, y) from I and provide estimates $(\hat{x}, \hat{y})$. Algorithms are usually assessed based on their mean squared error (MSE): $MSE(\hat{x}) =< (\hat{x} - x)^2 + (\hat{y} - y)^2 >$ where brackets denote statistical averaging. The MSE for coordinate x can be rewritten: $MSE(\hat{x}) = Var(\hat{x}) + B^2(\hat{x})$, where the variance $Var(\hat{x}) =< (\hat{x} - < \hat{x} >)^2$ is the random component of the errors, while the bias $B(\hat{x}) = x - < \hat{x} >$ is the systematic error (and likewise for y). The variance defines the 'precision' of an algorithm, while the bias defines the 'accuracy'. High precision algorithms tend to provide similar coordinates for different images of the same molecule, but these may have a large offset (bias) from the true value. High accuracy algorithms tend to find the correct position on average, but possibly with high dispersion (low precision), implying that individual localizations may still be far from the true location.



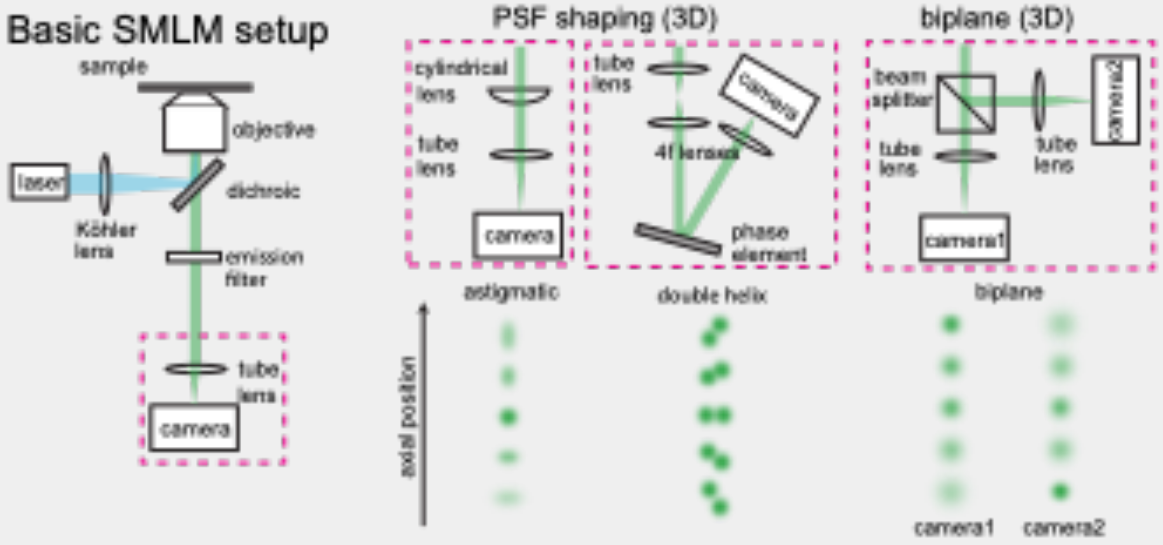
One usually considers algorithms without bias, so that $MSE(\hat{x}) = Var(\hat{x})$. The Cramer-Rao lower bound (CRLB) provides a lower limit to the variance (and hence precision) of any unbiased algorithm. Assuming for simplicity that the image depends only on x, the CRLB reads: $Var(\hat{x}) \geq -\left[< \frac{\partial^2}{\partial x^2} \ln p(I; x) >\right]^{-1}$ where $p(I; x)$ is the probability of observing I if the true coordinate is x ($p(I; x)$ is also called the likelihood). A handy formula can be derived under strongly idealized conditions, where the point spread function (PSF) is modeled as a Gaussian of standard deviation σ_0, the background and camera noise are neglected, and the exact coordinates of the N photons hitting the camera is recorded (i.e. ignoring pixelation). Under these assumptions, the CRLB reduces to: $Var(\hat{x}) \geq \sigma_0^2/N$, and the precision limit becomes: $\sigma_{loc} = \sigma(\hat{x}) \geq \sigma_0/\sqrt{N}$.

BOX 4: Three-dimensional (3D) SMLM

Biological structures are generally three-dimensional (3D), and should therefore be imaged in 3D with axial resolutions similar to those that can be achieved laterally. Innovations in optical setups exploiting point spread function (PSF) engineering[80,279] or multi-plane[280,281] detection have enabled precise localization of molecules in 3D, in samples up to several micrometers thick[102].

Methods with engineered PSFs exploit the fact that the 2D image of a fluorescent molecule depends not only on its lateral (x, y) coordinates but also on its axial coordinate z. By analyzing the 2D image pattern, the z coordinate can be estimated in addition to x and y. In this way, 3D super-resolution images can be reconstructed from 2D images obtained without refocusing. The most common approach exploits an astigmatic PSF, generated by inserting a single cylindrical lens into the imaging path[79,80,102] (see Figure). Other PSFs such as double helix (Figure), tetrapod or saddle point, which can be obtained using phase masks, deformable mirrors or other optical devices, can achieve larger axial range[102,279,282,283].

In setups with two or more focal planes (see Figure)[280,281,284], analyzing the relative intensities in different images of the same molecule also allows to compute z in addition to (x, y). In multifocal microscopy (MFM), a specialized diffractive grating is used to image several (e.g. up to 9) focal planes simultaneously on a single camera[281]. Combining MFM with SMLM allowed fast volumetric imaging of mitochondria in whole cells with high resolution[282].



PSF shaping or multi-plane detection divert photons for 3D encoding, resulting in a loss of localization precision. The theoretically achievable localization precision and axial range depend on the PSF shape, and can be calculated. Some PSFs have even been engineered to achieve theoretically optimal precisions over a given axial range[99,283]. Many software packages are now available for 3D SMLM with PSF engineering[99].

Acknowledgements

M. Lelek and C. Zimmer thank B. Lelandais for excellent comments on the manuscript. Work in the Zimmer lab is funded mainly by Institut Pasteur, Fondation pour la Recherche Médicale (grant DEQ 20150331762), Région Ile de France, and Agence Nationale de la Recherche. M. Lakadamyali acknowledges funding from the National Institutes of Health, National Institutes of General Medical Sciences (NIH/NIGMS) under the grant number RO1 GM133842-01. G. Beliu and M. Sauer acknowledge funding by the German Research Foundation (DFG, SA829/19-1) and the European Regional Development Fund (EFRE project ("Center for Personalized Molecular Immunotherapy"). F. Schueder and R. Jungmann acknowledge support by the German Research Foundation through the SFB1032 (project A11) and the Max Planck Society. This project was supported by the European Union's H2020 programme under the Marie Skłodowska-Curie grant BALTIC (J. Griffié) and ERC Piko (S. Manley).

Competing interests

Ralf Jungmann is cofounder of Ultivue, Inc. and Massive Photonics GmbH. Christophe Zimmer has an ongoing collaboration with Abbelight. All other authors declare no competing interests.

Glossary

- **Diffraction**: bending of light waves at the edges of an obstacle such as an aperture.
- **Point spread function (PSF):** the image of an infinitesimally small light source through the optical system.
- **Airy pattern:** a pattern of light featuring a central bright disk surrounded by increasingly dimmer concentric rings formed by diffraction from a circular aperture.
- **Total internal reflection (TIRF):** a configuration in which a strongly inclined laser beam is reflected by the coverslip, leaving only a thin (~200 nm) layer from the coverslip illuminated, strongly reducing background.
- **Highly inclined and laminated optical sheet (HILO):** a configuration in which the laser beam enters the sample at a sharp angle, allowing to reduce the background when imaging at a distance from the coverslip.
- **Noise:** Random fluctuations of the image pixel values.

- **Poisson noise (shot noise):** A type of statistical noise affecting photon counts and arising from the fact that photons are hitting pixels independently of each other with constant probability per unit time.

- **Cramer-Rao lower bound (CRLB):** A fundamental limit to the precision (variance) of any estimator without bias.

- **Ripley's K function:** A function computed from a set of points that helps reveal if points are uniformly randomly distributed or exhibit spatial clustering or dispersion.

- **Nyquist sampling:** sampling a continuous signal at twice the highest frequency allows to reconstruct it without loss of information.

- **Fourier ring correlation (FRC)**: a measure of image resolution computed from the cross-correlation between two independent noisy versions of the image in Fourier (frequency) space.

Related links:

- Single-Molecule Localization Microscopy Software Benchmarking: http://bigwww.epfl.ch/smlm

- Zenodo: an open access repository for research software and data: https://zenodo.org/

- FigShare: https://figshare.com/ an open access repository for figures, data sets and images

- Image Data Resource https://idr.openmicroscopy.org/ a public repository of imaging data

References:

1 Abbe, E. Beiträge zur Theorie des Mikroskops und der mikroskopischen Wahrnehmung. *Archiv für Mikroskopische Anatomie* **9**, 413-468, doi:10.1007/BF02956173 (1873).

2 Schermelleh, L. *et al.* Super-resolution microscopy demystified. *Nature Cell Biology* **21**, 72-84, doi:10.1038/s41556-018-0251-8 (2019).

3 Donnert, G. *et al.* Macromolecular-scale resolution in biological fluorescence microscopy. *Proceedings of the National Academy of Sciences* **103**, 11440-11445, doi:10.1073/pnas.0604965103 (2006).

4 Gustafsson, M. G. L. Surpassing the lateral resolution limit by a factor of two using structured illumination microscopy. *J Microsc* **198**, 82-87 (2000).

5 Heintzmann, R., Jovin, T. M. & Cremer, C. Saturated patterned excitation microscopy--a concept for optical resolution improvement. *J Opt Soc Am A Opt Image Sci Vis* **19**, 1599-1609 (2002).

6 Betzig, E. *et al.* Imaging intracellular fluorescent proteins at nanometer resolution. *Science* **313**, 1642-1645 (2006).

7 Hess, S. T., Girirajan, T. P. & Mason, M. D. Ultra-high resolution imaging by fluorescence photoactivation localization microscopy. *Biophys J* **91**, 4258-4272, doi:biophysj.106.091116 [pii] 10.1529/biophysj.106.091116 (2006).

8 Rust, M. J., Bates, M. & Zhuang, X. Sub-diffraction-limit imaging by stochastic optical reconstruction microscopy (STORM). *Nat Methods* **3**, 793-795, doi:nmeth929 [pii] 10.1038/nmeth929 (2006).

9 Heilemann, M. *et al.* Subdiffraction-resolution fluorescence imaging with conventional fluorescent probes. *Angew. Chemie. Int. Ed* **47**, 6172–6176 (2008).

10 Sharonov, A. & Hochstrasser, R. M. Wide-field subdiffraction imaging by accumulated binding of diffusing probes. *Proceedings of the National Academy of Sciences* **103**, 18911-18916, doi:10.1073/pnas.0609643104 (2006).

11 Lidke, K., Rieger, B., Jovin, T. & Heintzmann, R. Superresolution by localization of quantum dots using blinking statistics. *Opt Express* **13**, 7052-7062, doi:10.1364/opex.13.007052 (2005).

12 van Oijen, A. M., Kohler, J., Schmidt, J., Muller, M. & Brakenhoff, G. J. 3-Dimensional super-resolution by spectrally selective imaging. *Chem Phys Lett* **292**, 183-187, doi:Doi 10.1016/S0009-2614(98)00673-3 (1998).

13 Gordon, M. P., Ha, T. & Selvin, P. R. Single-molecule high-resolution imaging with photobleaching. *Proc Natl Acad Sci U S A* **101**, 6462-6465, doi:10.1073/pnas.0401638101 (2004).

14 Heilemann, M. *et al.* High-resolution colocalization of single dye molecules by fluorescence lifetime imaging microscopy. *Anal Chem* **74**, 3511-3517, doi:10.1021/ac025576g (2002).

15 Qu, X., Wu, D., Mets, L. & Scherer, N. F. Nanometer-localized multiple single-molecule fluorescence microscopy. *Proc Natl Acad Sci U S A* **101**, 11298-11303, doi:10.1073/pnas.0402155101 (2004).

16 Manley, S. *et al.* High-density mapping of single-molecule trajectories with photoactivated localization microscopy. *Nature Methods* **5**, 155-157, doi:10.1038/nmeth.1176 (2008).

17 Biteen, J. S. *et al.* Super-resolution imaging in live Caulobacter crescentus cells using photoswitchable EYFP. *Nat Methods* **5**, 947-949, doi:10.1038/nmeth.1258 (2008).

18 Folling, J. *et al.* Fluorescence nanoscopy by ground-state depletion and single-molecule return. *Nat Methods* **5**, 943-945, doi:10.1038/nmeth.1257 (2008).
19 Schnitzbauer, J., Strauss, M. T., Schlichthaerle, T., Schueder, F. & Jungmann, R. Super-resolution microscopy with DNA-PAINT. *Nat Protoc* **12**, 1198-1228, doi:10.1038/nprot.2017.024 (2017).
20 Bintu, B. *et al.* Super-resolution chromatin tracing reveals domains and cooperative interactions in single cells. *Science* **362**, eaau1783, doi:10.1126/science.aau1783 (2018).
21 Weisenburger, S. *et al.* Cryogenic optical localization provides 3D protein structure data with Angstrom resolution. *Nat Methods* **14**, 141-144, doi:10.1038/nmeth.4141 (2017).
22 Klein, T., Proppert, S. & Sauer, M. Eight years of single-molecule localization microscopy. *Histochem Cell Biol* **141**, 561-575, doi:10.1007/s00418-014-1184-3 (2014).
23 Bates, M., Blosser, T. R. & Zhuang, X. Short-range spectroscopic ruler based on a single-molecule optical switch. *Phys Rev Lett* **94**, 108101, doi:10.1103/PhysRevLett.94.108101 (2005).
24 Heilemann, M., Margeat, E., Kasper, R., Sauer, M. & Tinnefeld, P. Carbocyanine Dyes as Efficient Reversible Single-Molecule Optical Switch. *J. Am. Chem. Soc.* **127**, 3801-3806, doi:10.1021/ja044686x
10.1021/ja044686x</p> (2005).
25 Lin, Y. *et al.* Quantifying and optimizing single-molecule switching nanoscopy at high speeds. *PLoS One* **10**, e0128135, doi:10.1371/journal.pone.0128135 (2015).
26 Diekmann, R. *et al.* Optimizing imaging speed and excitation intensity for single-molecule localization microscopy. *Nat Methods* **17**, 909-912, doi:10.1038/s41592-020-0918-5 (2020).
27 van de Linde, S. *et al.* Direct stochastic optical reconstruction microscopy with standard fluorescent probes. *Nature protocols* **6**, 991-1009, doi:10.1038/nprot.2011.336 (2011).
28 Wombacher, R. *et al.* Live-cell super-resolution imaging with trimethoprim conjugates. *Nature Methods* **7**, 717-719 (2010).
29 Andresen, M. *et al.* Structural basis for reversible photoswitching in Dronpa. *Proceedings of the National Academy of Sciences* **104**, 13005, doi:10.1073/pnas.0700629104 (2007).
30 Bossi, M. *et al.* Multicolor Far-Field Fluorescence Nanoscopy through Isolated Detection of Distinct Molecular Species. *Nano Lett.* **8**, 2463-2468, doi:10.1021/nl801471d
10.1021/nl801471d</p> (2008).
31 Grimm, J. B. *et al.* Bright photoactivatable fluorophores for single-molecule imaging. *Nat Methods* **13**, 985-988, doi:10.1038/nmeth.4034 (2016).
32 Michie, M. S. *et al.* Cyanine Conformational Restraint in the Far-Red Range. *J Am Chem Soc* **139**, 12406-12409, doi:10.1021/jacs.7b07272 (2017).
33 Lukyanov, K. A., Chudakov, D. M., Lukyanov, S. & Verkhusha, V. V. Photoactivatable fluorescent proteins. *Nature Reviews Molecular Cell Biology* **6**, 885-890, doi:10.1038/nrm1741 (2005).
34 Shroff, H., Galbraith, C. G., Galbraith, J. A. & Betzig, E. Live-cell photoactivated localization microscopy of nanoscale adhesion dynamics. *Nature Methods* **5**, 417-423, doi:10.1038/nmeth.1202 (2008).
35 Wang, S., Moffitt, J. R., Dempsey, G. T., Xie, X. S. & Zhuang, X. Characterization and development of photoactivatable fluorescent proteins for single-molecule-based superresolution imaging. *Proc Natl Acad Sci U S A* **111**, 8452-8457, doi:10.1073/pnas.1406593111 (2014).
36 Turkowyd, B., Virant, D. & Endesfelder, U. From single molecules to life: microscopy at the nanoscale. *Anal Bioanal Chem* **408**, 6885-6911, doi:10.1007/s00216-016-9781-8 (2016).

37 McEvoy, A. L. *et al.* mMaple: a photoconvertible fluorescent protein for use in multiple imaging modalities. *PLoS One* **7**, e51314, doi:10.1371/journal.pone.0051314 (2012).

38 Uno, S. N. *et al.* A spontaneously blinking fluorophore based on intramolecular spirocyclization for live-cell super-resolution imaging. *Nat Chem* **6**, 681-689, doi:10.1038/nchem.2002 (2014).

39 Takakura, H. *et al.* Long time-lapse nanoscopy with spontaneously blinking membrane probes. *Nat Biotechnol* **35**, 773-780, doi:10.1038/nbt.3876 (2017).

40 Uno, S. N., Kamiya, M., Morozumi, A. & Urano, Y. A green-light-emitting, spontaneously blinking fluorophore based on intramolecular spirocyclization for dual-colour super-resolution imaging. *Chem Commun (Camb)* **54**, 102-105, doi:10.1039/c7cc07783a (2017).

41 Macdonald, P. J. *et al.* Rhodamine-Derived Fluorescent Dye with Inherent Blinking Behavior for Super-Resolution Imaging. *Anal Chem* **90**, 9165-9173, doi:10.1021/acs.analchem.8b01645 (2018).

42 Giannone, G. *et al.* Dynamic superresolution imaging of endogenous proteins on living cells at ultra-high density. *Biophys J* **99**, 1303-1310, doi:10.1016/j.bpj.2010.06.005 (2010).

43 Jungmann, R. *et al.* Single-molecule kinetics and super-resolution microscopy by fluorescence imaging of transient binding on DNA origami. *Nano Lett* **10**, 4756-4761, doi:10.1021/nl103427w (2010).

44 Dai, M., Jungmann, R. & Yin, P. Optical imaging of individual biomolecules in densely packed clusters. *Nat Nanotechnol* **11**, 798-807, doi:10.1038/nnano.2016.95 (2016).

45 Shcherbakova, D. M., Sengupta, P., Lippincott-Schwartz, J. & Verkhusha, V. V. Photocontrollable fluorescent proteins for superresolution imaging. *Annu Rev Biophys* **43**, 303-329, doi:10.1146/annurev-biophys-051013-022836 (2014).

46 Thorn, K. Genetically encoded fluorescent tags. *Mol Biol Cell* **28**, 848-857, doi:10.1091/mbc.E16-07-0504 (2017).

47 Rodriguez, E. A. *et al.* The Growing and Glowing Toolbox of Fluorescent and Photoactive Proteins. *Trends Biochem Sci* **42**, 111-129, doi:10.1016/j.tibs.2016.09.010 (2017).

48 Li, H. & Vaughan, J. C. Switchable Fluorophores for Single-Molecule Localization Microscopy. *Chem Rev* **118**, 9412-9454, doi:10.1021/acs.chemrev.7b00767 (2018).

49 Fernandez-Suarez, M. & Ting, A. Y. Fluorescent probes for super-resolution imaging in living cells. *Nat Rev Mol Cell Biol* **9**, 929-943, doi:10.1038/nrm2531 (2008).

50 Ries, J., Kaplan, C., Platonova, E., Eghlidi, H. & Ewers, H. A simple, versatile method for GFP-based super-resolution microscopy via nanobodies. *Nat Methods* **9**, 582-584, doi:10.1038/nmeth.1991 (2012).

51 Herce, H. D. *et al.* Cell-permeable nanobodies for targeted immunolabelling and antigen manipulation in living cells. *Nat Chem* **9**, 762-771, doi:10.1038/nchem.2811 (2017).

52 Conic, S. *et al.* Imaging of native transcription factors and histone phosphorylation at high resolution in live cells. *Journal of Cell Biology* **217**, 1537-1552, doi:10.1083/jcb.201709153 (2018).

53 Schnell, U., Dijk, F., Sjollema, K. A. & Giepmans, B. N. Immunolabeling artifacts and the need for live-cell imaging. *Nat Methods* **9**, 152-158, doi:10.1038/nmeth.1855 (2012).

54 Yan, Q. & Bruchez, M. P. Advances in chemical labeling of proteins in living cells. *Cell Tissue Res* **360**, 179-194, doi:10.1007/s00441-015-2145-4 (2015).

55 Liss, V., Barlag, B., Nietschke, M. & Hensel, M. Self-labelling enzymes as universal tags for fluorescence microscopy, super-resolution microscopy and electron microscopy. *Sci Rep* **5**, 17740, doi:10.1038/srep17740 (2015).

56 Lelek, M., Di Nunzio, F. & Zimmer, C. in *Exocytosis and Endocytosis Methods in Molecular Biology* (ed Andrei I. Ivanov) 183-193 (Springer New York, 2014).

57 Klein, T. *et al.* Live-cell dSTORM with SNAP-tag fusion proteins. *Nat Methods* **8**, 7-9, doi:nmeth0111-7b [pii] 10.1038/nmeth0111-7b (2011).

58 Xu, K., Zhong, G. & Zhuang, X. Actin, Spectrin, and Associated Proteins Form a Periodic Cytoskeletal Structure in Axons. *Science* **339** (2013).

59 Wijesooriya, C. S. *et al.* A Photoactivatable BODIPY Probe for Localization-Based Super-Resolution Cellular Imaging. *Angew Chem Int Ed Engl* **57**, 12685-12689, doi:10.1002/anie.201805827 (2018).

60 Shim, S. H. *et al.* Super-resolution fluorescence imaging of organelles in live cells with photoswitchable membrane probes. *Proceedings of the National Academy of Sciences of the United States of America* **109**, 13978-13983, doi:10.1073/pnas.1201882109 (2012).

61 Neubert, F. *et al.* Bioorthogonal Click Chemistry Enables Site-specific Fluorescence Labeling of Functional NMDA Receptors for Super-Resolution Imaging. *Angew Chem Int Ed Engl* **57**, 16364-16369, doi:10.1002/anie.201808951 (2018).

62 Beliu, G. *et al.* Bioorthogonal labeling with tetrazine-dyes for super-resolution microscopy. *Commun Biol* **2**, 261, doi:10.1038/s42003-019-0518-z (2019).

63 Lang, K. & Chin, J. W. Cellular incorporation of unnatural amino acids and bioorthogonal labeling of proteins. *Chem Rev* **114**, 4764-4806, doi:10.1021/cr400355w (2014).

64 Lew, M. D. *et al.* Three-dimensional superresolution colocalization of intracellular protein superstructures and the cell surface in live Caulobacter crescentus. *Proc Natl Acad Sci U S A* **108**, E1102-1110, doi:10.1073/pnas.1114444108 (2011).

65 Spahn, C. K. *et al.* A toolbox for multiplexed super-resolution imaging of the E. coli nucleoid and membrane using novel PAINT labels. *Sci Rep* **8**, 14768, doi:10.1038/s41598-018-33052-3 (2018).

66 Agasti, S. S. *et al.* DNA-barcoded labeling probes for highly multiplexed Exchange-PAINT imaging. *Chem Sci* **8**, 3080-3091, doi:10.1039/c6sc05420j (2017).

67 Schlichthaerle, T. *et al.* Direct Visualization of Single Nuclear Pore Complex Proteins Using Genetically-Encoded Probes for DNA-PAINT. *Angew Chem Int Ed Engl* **58**, 13004-13008, doi:10.1002/anie.201905685 (2019).

68 Sograte-Idrissi, S. *et al.* Circumvention of common labelling artefacts using secondary nanobodies. *Nanoscale* **12**, 10226-10239, doi:10.1039/d0nr00227e (2020).

69 Schlichthaerle, T. *et al.* Site-Specific Labeling of Affimers for DNA-PAINT Microscopy. *Angew Chem Int Ed Engl* **57**, 11060-11063, doi:10.1002/anie.201804020 (2018).

70 Strauss, S. *et al.* Modified aptamers enable quantitative sub-10-nm cellular DNA-PAINT imaging. *Nat Methods* **15**, 685-688, doi:10.1038/s41592-018-0105-0 (2018).

71 Richter, K. N. *et al.* Glyoxal as an alternative fixative to formaldehyde in immunostaining and super-resolution microscopy. *EMBO J* **37**, 139-159, doi:10.15252/embj.201695709 (2018).

72 Tanaka, K. A. *et al.* Membrane molecules mobile even after chemical fixation. *Nat Methods* **7**, 865-866, doi:10.1038/nmeth.f.314 (2010).

73 Baumgart, F. *et al.* Varying label density allows artifact-free analysis of membrane-protein nanoclusters. *Nat Methods* **13**, 661-664, doi:10.1038/nmeth.3897 (2016).

74 Tuijtel, M. W., Koster, A. J., Jakobs, S., Faas, F. G. A. & Sharp, T. H. Correlative cryo super-resolution light and electron microscopy on mammalian cells using fluorescent proteins. *Sci Rep* **9**, 1369, doi:10.1038/s41598-018-37728-8 (2019).

75 Kopek, B. G. *et al.* Diverse protocols for correlative super-resolution fluorescence imaging and electron microscopy of chemically fixed samples. *Nat Protoc* **12**, 916-946, doi:10.1038/nprot.2017.017 (2017).

76 Waldchen, S., Lehmann, J., Klein, T., van de Linde, S. & Sauer, M. Light-induced cell damage in live-cell super-resolution microscopy. *Sci Rep* **5**, 15348, doi:10.1038/srep15348 (2015).

77 Holm, T. *et al.* A blueprint for cost-efficient localization microscopy. *ChemPhysChem* **15**, 651-654 (2014).
78 Kwakwa, K. *et al.* easySTORM: a robust, lower-cost approach to localisation and TIRF microscopy. *Journal of Biophotonics* **9**, 948-957 (2016).
79 Henriques, R. *et al.* QuickPALM: 3D real-time photoactivation nanoscopy image processing in ImageJ. *Nature Methods* **7**, 339-340 (2010).
80 Huang, B., Wang, W., Bates, M. & Zhuang, X. Three-dimensional super-resolution imaging by stochastic optical reconstruction microscopy. *Science* **319**, 810-813, doi:10.1126/science.1153529 (2008).
81 Mashanov, G. I., Tacon, D., Knight, A. E., Peckham, M. & Molloy, J. E. Visualizing single molecules inside living cells using total internal reflection fluorescence microscopy. *Methods* **29**, 142-152, doi:10.1016/s1046-2023(02)00305-5 (2003).
82 Tokunaga, M., Imamoto, N. & Sakata-Sogawa, K. Highly inclined thin illumination enables clear single-molecule imaging in cells. *Nature methods* **5**, 159-161 (2008).
83 Thompson, R. E., Larson, D. R. & Webb, W. W. Precise nanometer localization analysis for individual fluorescent probes. *Biophys J* **82**, 2775-2783 (2002).
84 Ober, R. J., Ram, S. & Ward, E. S. Localization Accuracy in Single-Molecule Microscopy. *Biophysical journal* **86**, 1185-1200 (2004).
85 Holden, S. J. *et al.* High throughput 3D super-resolution microscopy reveals Caulobacter crescentus in vivo Z-ring organization. *Proceedings of the National Academy of Sciences of the United States of America* **111**, 4566-4571 (2014).
86 Kechkar, A., Nair, D., Heilemann, M., Choquet, D. & Sibarita, J. B. Real-Time Analysis and Visualization for Single-Molecule Based Super-Resolution Microscopy. *PLoS ONE* **8**, doi:10.1371/journal.pone.0062918 (2013).
87 Mund, M. *et al.* Systematic Nanoscale Analysis of Endocytosis Links Efficient Vesicle Formation to Patterned Actin Nucleation. *Cell* **174**, 884-896.e817, doi:10.1016/j.cell.2018.06.032 (2018).
88 Fox-Roberts, P. *et al.* Local dimensionality determines imaging speed in localization microscopy. *Nat Commun* **8**, 13558-13558, doi:10.1038/ncomms13558 (2017).
89 Legant, W. R. *et al.* High-density three-dimensional localization microscopy across large volumes. *Nature Methods* **13**, 359-365, doi:10.1038/nmeth.3797 (2016).
90 Jones, S. A., Shim, S. H., He, J. & Zhuang, X. Fast, three-dimensional super-resolution imaging of live cells. *Nat Methods* **8**, 499-505, doi:nmeth.1605 [pii] 10.1038/nmeth.1605 (2011).
91 Gelles, J., Schnapp, B. J. & Sheetz, M. P. Tracking kinesin-driven movements with nanometre-scale precision. *Nature* **331**, 450-453 (1988).
92 Sergé, A., Bertaux, N., Rigneault, H. & Marguet, D. Dynamic multiple-target tracing to probe spatiotemporal cartography of cell membranes. *Nat Methods* **5**, 687-694, doi:nmeth.1233 [pii] 10.1038/nmeth.1233 (2008).
93 Elf, J. & Barkefors, I. Single-Molecule Kinetics in Living Cells. *Annu Rev Biochem* **88**, 635-659, doi:10.1146/annurev-biochem-013118-110801 (2019).
94 Ovesny, M., Kiek, P., Borkovec, J., Vindrych, Z. & Hagen, G. M. ThunderSTORM: a comprehensive ImageJ plug-in for PALM and STORM data analysis and super-resolution imaging. *Bioinformatics* **30**, 2389-2390, doi:10.1093/bioinformatics/btu202 (2014).
95 Cheng, C.-Y. & Hsieh, C.-L. Background Estimation and Correction for High-Precision Localization Microscopy. *ACS Photonics* **4**, 1730-1739, doi:10.1021/acsphotonics.7b00238 (2017).
96 Kay, S. M. *Fundamentals of Statistical Signal Processing, Volume 2: Detection Theory*. (Prentice Hall PTR, 1998).
97 Kay, S. M. *Fundamentals of statistical signal processing: estimation theory*. (1993).

98 Mortensen, K. I., Churchman, L. S., Spudich, J. A. & Flyvbjerg, H. Optimized localization analysis for single-molecule tracking and super-resolution microscopy. *Nature Methods* **7**, 377-381, doi:10.1038/nmeth.1447 (2010).
99 Sage, D. *et al.* Super-resolution fight club: assessment of 2D and 3D single-molecule localization microscopy software. *Nature Methods* **16**, 387-395, doi:10.1038/s41592-019-0364-4 (2019).
100 Small, A. & Stahlheber, S. Fluorophore localization algorithms for super-resolution microscopy. *Nature Methods* **11**, 267-279, doi:10.1038/nmeth.2844 (2014).
101 Li, Y. *et al.* Real-time 3D single-molecule localization using experimental point spread functions. *Nat Methods* **15**, 367-369, doi:10.1038/nmeth.4661 (2018).
102 Aristov, A., Lelandais, B., Rensen, E. & Zimmer, C. ZOLA-3D allows flexible 3D localization microscopy over an adjustable axial range. *Nat Commun* **9**, 2409, doi:10.1038/s41467-018-04709-4 (2018).
103 Sage, D. *et al.* Quantitative evaluation of software packages for single-molecule localization microscopy. *Nature Methods* **12**, 717-724, doi:10.1038/nmeth.3442 (2015).
104 Annibale, P., Vanni, S., Scarselli, M., Rothlisberger, U. & Radenovic, A. Identification of clustering artifacts in photoactivated localization microscopy. *Nature Methods* **8**, 527-528, doi:10.1038/nmeth.1627 (2011).
105 Sengupta, P. *et al.* Probing protein heterogeneity in the plasma membrane using PALM and pair correlation analysis. *Nat Methods* **8**, 969-975, doi:Doi 10.1038/Nmeth.1704 (2011).
106 Rubin-Delanchy, P. *et al.* Bayesian cluster identification in single-molecule localization microscopy data. *Nature Methods* **12**, 1072-1076, doi:10.1038/nmeth.3612 (2015).
107 Khater, I. M., Nabi, I. R. & Hamarneh, G. A Review of Super-Resolution Single-Molecule Localization Microscopy Cluster Analysis and Quantification Methods. *Patterns* **1**, 100038, doi:https://doi.org/10.1016/j.patter.2020.100038 (2020).
108 Levet, F. *et al.* SR-Tesseler: a method to segment and quantify localization-based super-resolution microscopy data. *Nature Methods* **12**, 1065-1071, doi:10.1038/nmeth.3579 (2015).
109 Durisic, N., Laparra-Cuervo, L., Sandoval-Alvarez, A., Borbely, J. S. & Lakadamyali, M. Single-molecule evaluation of fluorescent protein photoactivation efficiency using an in vivo nanotemplate. *Nat Methods* **11**, 156-162, doi:10.1038/nmeth.2784 (2014).
110 Bohrer, C. H. *et al.* A Pairwise Distance Distribution Correction (DDC) algorithm to eliminate blinking-caused artifacts in super-resolution microscopy. *bioRxiv*, 768051, doi:10.1101/768051 (2020).
111 Veatch, S. L. *et al.* Correlation functions quantify super-resolution images and estimate apparent clustering due to over-counting. *PLoS One* **7**, e31457, doi:10.1371/journal.pone.0031457 (2012).
112 Zanacchi, F. C. *et al.* A DNA origami platform for quantifying protein copy number in super-resolution. *Nat Methods* **14**, 789-792, doi:10.1038/nmeth.4342 (2017).
113 Thevathasan, J. V. *et al.* Nuclear pores as versatile reference standards for quantitative superresolution microscopy. *Nature Methods* **16**, 1045-1053, doi:10.1038/s41592-019-0574-9 (2019).
114 Finan, K., Raulf, A. & Heilemann, M. A set of homo-oligomeric standards allows accurate protein counting. *Angew Chem Int Ed Engl* **54**, 12049-12052, doi:10.1002/anie.201505664 (2015).
115 Rollins, G. C., Shin, J. Y., Bustamante, C. & Presse, S. Stochastic approach to the molecular counting problem in superresolution microscopy. *Proc Natl Acad Sci U S A* **112**, E110-118, doi:10.1073/pnas.1408071112 (2015).
116 Lee, S.-H., Shin, J. Y., Lee, A. & Bustamante, C. Counting single photoactivatable fluorescent molecules by photoactivated localization microscopy (PALM). *Proceedings of*

the National Academy of Sciences of the United States of America **109**, 17436-17441, doi:10.1073/pnas.1215175109 (2012).

117 Jungmann, R. *et al.* Quantitative super-resolution imaging with qPAINT. *Nat Methods* **13**, 439-442, doi:10.1038/nmeth.3804 (2016).

118 Salas, D. *et al.* Angular reconstitution-based 3D reconstructions of nanomolecular structures from superresolution light-microscopy images. *Proceedings of the National Academy of Sciences* **114**, 9273-9278, doi:10.1073/pnas.1704908114 (2017).

119 Sieben, C., Banterle, N., Douglass, K. M., Gönczy, P. & Manley, S. Multicolor single-particle reconstruction of protein complexes. *Nature Methods* **15**, 777-780, doi:10.1038/s41592-018-0140-x (2018).

120 Szymborska, A. *et al.* Nuclear pore scaffold structure analyzed by super-resolution microscopy and particle averaging. *Science (New York, N.Y.)* **341**, 655-658, doi:10.1126/science.1240672 (2013).

121 Bolte, S. & Cordelières, F. P. A guided tour into subcellular colocalization analysis in light microscopy. *Journal of microscopy* **224**, 213-232 (2006).

122 Lagache, T. *et al.* Mapping molecular assemblies with fluorescence microscopy and object-based spatial statistics. *Nat Commun* **9**, 698, doi:10.1038/s41467-018-03053-x (2018).

123 Levet, F. *et al.* A tessellation-based colocalization analysis approach for single-molecule localization microscopy. *Nat Commun* **10**, 2379, doi:10.1038/s41467-019-10007-4 (2019).

124 Malkusch, S. *et al.* Coordinate-based colocalization analysis of single-molecule localization microscopy data. *Histochemistry and Cell Biology* **137**, 1-10, doi:10.1007/s00418-011-0880-5 (2012).

125 Monnier, N. *et al.* Bayesian Approach to MSD-Based Analysis of Particle Motion in Live Cells. *Biophysical Journal* **103**, 616-626 (2012).

126 Beheiry, M. E., Dahan, M. & Masson, J.-B. InferenceMAP: mapping of single-molecule dynamics with Bayesian inference. *Nature Methods* **12**, 594-595, doi:10.1038/nmeth.3441 (2015).

127 Martin, D. S., Forstner, M. B. & Kas, J. A. Apparent subdiffusion inherent to single particle tracking. *Biophys J* **83**, 2109-2117, doi:10.1016/S0006-3495(02)73971-4 (2002).

128 Masson, J. B. *et al.* Mapping the energy and diffusion landscapes of membrane proteins at the cell surface using high-density single-molecule imaging and Bayesian inference: application to the multiscale dynamics of glycine receptors in the neuronal membrane. *Biophys J* **106**, 74-83, doi:10.1016/j.bpj.2013.10.027 (2014).

129 Manzo, C. & Garcia-Parajo, M. F. A review of progress in single particle tracking: from methods to biophysical insights. *Rep Prog Phys* **78**, 124601, doi:10.1088/0034-4885/78/12/124601 (2015).

130 Peters, R., Griffié, J., Burn, G. L., Williamson, D. J. & Owen, D. M. Quantitative fibre analysis of single-molecule localization microscopy data. *Scientific Reports* **8**, 10418, doi:10.1038/s41598-018-28691-5 (2018).

131 Zhang, Z., Nishimura, Y. & Kanchanawong, P. Extracting microtubule networks from superresolution single-molecule localization microscopy data. *Molecular Biology of the Cell* **28**, 333-345, doi:10.1091/mbc.E16-06-0421 (2017).

132 Gyparaki, M. T. *et al.* Tau forms oligomeric complexes on microtubules that are distinct from pathological oligomers in disease. *bioRxiv* (2020).

133 Nicovich, P. R., Owen, D. M. & Gaus, K. Turning single-molecule localization microscopy into a quantitative bioanalytical tool. *Nature Protocols* **12**, 453-460, doi:10.1038/nprot.2016.166 (2017).

134 Deschout, H., Shivanandan, A., Annibale, P., Scarselli, M. & Radenovic, A. Progress in quantitative single-molecule localization microscopy. *Histochemistry and cell biology* **142**, doi:10.1007/s00418-014-1217-y (2014).
135 Rowley, M. J. & Corces, V. G. Organizational principles of 3D genome architecture. *Nature Reviews Genetics* **19**, 789-800, doi:10.1038/s41576-018-0060-8 (2018).
136 Lakadamyali, M. & Cosma, M. P. Visualizing the genome in high resolution challenges our textbook understanding. *Nature Methods* **17**, 371-379, doi:10.1038/s41592-020-0758-3 (2020).
137 Nozaki, T. *et al.* Dynamic Organization of Chromatin Domains Revealed by Super-Resolution Live-Cell Imaging. *Mol Cell* **67**, 282-293 e287, doi:10.1016/j.molcel.2017.06.018 (2017).
138 Gomez-Garcia, P. A. *et al.* Mesoscale Modeling and Single-Nucleosome Tracking Reveal Remodeling of Clutch Folding and Dynamics in Stem Cell Differentiation. *Cell Rep* **34**, 108614, doi:10.1016/j.celrep.2020.108614 (2021).
139 Ricci, M. A., Manzo, C., García-Parajo, M. F., Lakadamyali, M. & Cosma, M. P. Chromatin fibers are formed by heterogeneous groups of nucleosomes in vivo. *Cell* **160**, 1145-1158, doi:10.1016/j.cell.2015.01.054 (2015).
140 Otterstrom, J. *et al.* Super-resolution microscopy reveals how histone tail acetylation affects DNA compaction within nucleosomes in vivo. *Nucleic Acids Res* **47**, 8470-8484, doi:10.1093/nar/gkz593 (2019).
141 Xu, J. *et al.* Super-Resolution Imaging of Higher-Order Chromatin Structures at Different Epigenomic States in Single Mammalian Cells. *Cell Reports* **24**, 873-882, doi:10.1016/j.celrep.2018.06.085 (2018).
142 Zessin, P. J., Finan, K. & Heilemann, M. Super-resolution fluorescence imaging of chromosomal DNA. *J Struct Biol* **177**, 344-348, doi:10.1016/j.jsb.2011.12.015 (2012).
143 Boettiger, A. N. *et al.* Super-resolution imaging reveals distinct chromatin folding for different epigenetic states. *Nature* **529**, 418-422, doi:10.1038/nature16496 (2016).
144 Beagan, J. A. & Phillips-Cremins, J. E. On the existence and functionality of topologically associating domains. *Nature Genetics* **52**, 8-16, doi:10.1038/s41588-019-0561-1 (2020).
145 Nir, G. *et al.* Walking along chromosomes with super-resolution imaging, contact maps, and integrative modeling. *PLoS Genetics* **14**, e1007872-e1007872, doi:10.1371/journal.pgen.1007872 (2018).
146 Boettiger, A. & Murphy, S. Advances in Chromatin Imaging at Kilobase-Scale Resolution. *Trends Genet* **36**, 273-287, doi:10.1016/j.tig.2019.12.010 (2020).
147 Cisse, I. I. *et al.* Real-time dynamics of RNA polymerase II clustering in live human cells. *Science (New York, N.Y.)* **341**, 664-667, doi:10.1126/science.1239053 (2013).
148 Cho, W. K. *et al.* RNA Polymerase II cluster dynamics predict mRNA output in living cells. *eLife* **5**, doi:10.7554/eLife.13617 (2016).
149 Cho, W. K. *et al.* Mediator and RNA polymerase II clusters associate in transcription-dependent condensates. *Science* **361**, 412-415, doi:10.1126/science.aar4199 (2018).
150 Hansen, A. S., Pustova, I., Cattoglio, C., Tjian, R. & Darzacq, X. CTCF and cohesin regulate chromatin loop stability with distinct dynamics. *eLife* **6**, e25776, doi:10.7554/eLife.25776 (2017).
151 Wani, A. H. *et al.* Chromatin topology is coupled to Polycomb group protein subnuclear organization. *Nat Commun* **7**, 1-13, doi:10.1038/ncomms10291 (2016).
152 Löschberger, A. *et al.* Super-resolution imaging visualizes the eightfold symmetry of gp210 proteins around the nuclear pore complex and resolves the central channel with nanometer resolution. *Journal of cell science* **125**, 570-575, doi:10.1242/jcs.098822 (2012).

153 Broeken, J. *et al.* Resolution improvement by 3D particle averaging in localization microscopy. *Methods and applications in fluorescence* **3**, 014003-014003, doi:10.1088/2050-6120/3/1/014003 (2015).
154 Mudumbi, K. C. *et al.* Nucleoplasmic signals promote directed transmembrane protein import simultaneously via multiple channels of nuclear pores. *Nat Commun* **11**, 1-14, doi:10.1038/s41467-020-16033-x (2020).
155 Zhu, L., Zhang, W., Elnatan, D. & Huang, B. Faster STORM using compressed sensing. *Nature Methods* **9**, 721-723, doi:10.1038/nmeth.1978 (2012).
156 Bálint, Š., Vilanova, I. V., Álvarez, Á. S. & Lakadamyali, M. Correlative live-cell and superresolution microscopy reveals cargo transport dynamics at microtubule intersections. *Proceedings of the National Academy of Sciences of the United States of America* **110**, 3375-3380, doi:10.1073/pnas.1219206110 (2013).
157 Verdeny-Vilanova, I. *et al.* Vol. 130 1904-1916 (Company of Biologists Ltd, 2017).
158 Mohan, N., Sorokina, E. M., Verdeny, I. V., Alvarez, A. S. & Lakadamyali, M. Detyrosinated microtubules spatially constrain lysosomes facilitating lysosome-autophagosome fusion. *Journal of Cell Biology* **218**, 632-643, doi:10.1083/jcb.201807124 (2019).
159 Jakobs, S. & Wurm, C. A. Vol. 20 9-15 (Elsevier Ltd, 2014).
160 Brown, T. A. *et al.* Superresolution Fluorescence Imaging of Mitochondrial Nucleoids Reveals Their Spatial Range, Limits, and Membrane Interaction. *Molecular and Cellular Biology* **31**, 4994-5010, doi:10.1128/mcb.05694-11 (2011).
161 Nixon-Abell, J. *et al.* Increased spatiotemporal resolution reveals highly dynamic dense tubular matrices in the peripheral ER. *Science* **354**, doi:10.1126/science.aaf3928 (2016).
162 Karathanasis, C. *et al.* Single-molecule imaging reveals the oligomeric state of functional TNFalpha-induced plasma membrane TNFR1 clusters in cells. *Sci Signal* **13**, doi:10.1126/scisignal.aax5647 (2020).
163 Neumann, J. *et al.* Nanoscale distribution of TLR4 on primary human macrophages stimulated with LPS and ATI. *Nanoscale* **11**, 9769-9779, doi:10.1039/c9nr00943d (2019).
164 Nerreter, T. *et al.* Super-resolution microscopy reveals ultra-low CD19 expression on myeloma cells that triggers elimination by CD19 CAR-T. *Nat Commun* **10**, 3137, doi:10.1038/s41467-019-10948-w (2019).
165 Lillemeier, B. F. *et al.* TCR and Lat are expressed on separate protein islands on T cell membranes and concatenate during activation. *Nature Immunology* **11**, 90-96, doi:10.1038/ni.1832 (2010).
166 Pageon, S. V. *et al.* Functional role of T-cell receptor nanoclusters in signal initiation and antigen discrimination. *Proceedings of the National Academy of Sciences of the United States of America* **113**, E5454-E5463, doi:10.1073/pnas.1607436113 (2016).
167 Rossboth, B. *et al.* TCRs are randomly distributed on the plasma membrane of resting antigen-experienced T cells. *Nature Immunology* **19**, 821-827, doi:10.1038/s41590-018-0162-7 (2018).
168 Stone, M. B., Shelby, S. A. & Veatch, S. L. Super-Resolution Microscopy: Shedding Light on the Cellular Plasma Membrane. *Chem Rev* **117**, 7457-7477, doi:10.1021/acs.chemrev.6b00716 (2017).
169 Kanchanawong, P. *et al.* Nanoscale architecture of integrin-based cell adhesions. *Nature* **468**, 580-584, doi:10.1038/nature09621 (2010).
170 Liu, J. *et al.* Talin determines the nanoscale architecture of focal adhesions. *Proceedings of the National Academy of Sciences of the United States of America* **112**, E4864-E4873, doi:10.1073/pnas.1512025112 (2015).

171 Dani, A., Huang, B., Bergan, J., Dulac, C. & Zhuang, X. Superresolution Imaging of Chemical Synapses in the Brain. *Neuron* **68**, 843-856, doi:10.1016/j.neuron.2010.11.021 (2010).
172 Ehmann, N. *et al.* Quantitative super-resolution imaging of Bruchpilot distinguishes active zone states. *Nat Commun* **5**, 1-12, doi:10.1038/ncomms5650 (2014).
173 Nair, D. *et al.* Super-resolution imaging reveals that AMPA receptors inside synapses are dynamically organized in nanodomains regulated by PSD95. *Journal of Neuroscience* **33**, 13204-13224, doi:10.1523/JNEUROSCI.2381-12.2013 (2013).
174 Kellermayer, B. *et al.* Differential Nanoscale Topography and Functional Role of GluN2-NMDA Receptor Subtypes at Glutamatergic Synapses. *Neuron* **100**, 106-119.e107, doi:10.1016/j.neuron.2018.09.012 (2018).
175 Ladépêche, L. *et al.* NMDA Receptor Autoantibodies in Autoimmune Encephalitis Cause a Subunit-Specific Nanoscale Redistribution of NMDA Receptors. *Cell Reports* **23**, 3759-3768, doi:10.1016/j.celrep.2018.05.096 (2018).
176 Siddig, S. *et al.* Super-resolution imaging reveals the nanoscale organization of metabotropic glutamate receptors at presynaptic active zones. *Sci Adv* **6**, eaay7193, doi:10.1126/sciadv.aay7193 (2020).
177 Lehmann, M. *et al.* Quantitative multicolor super-resolution microscopy reveals tetherin HIV-1 interaction. *PLoS Pathog* **7**, e1002456, doi:10.1371/journal.ppat.1002456 (2011).
178 Chojnacki, J. & Eggeling, C. Super-resolution fluorescence microscopy studies of human immunodeficiency virus. *Retrovirology* **15**, 41, doi:10.1186/s12977-018-0424-3 (2018).
179 Pak, A. J. *et al.* Immature HIV-1 lattice assembly dynamics are regulated by scaffolding from nucleic acid and the plasma membrane. *Proc Natl Acad Sci U S A* **114**, E10056-E10065, doi:10.1073/pnas.1706600114 (2017).
180 Lelek, M. *et al.* Superresolution imaging of HIV in infected cells with FlAsH-PALM. *Proc Natl Acad Sci U S A* **109**, 8564-8569, doi:10.1073/pnas.1013267109 (2012).
181 Van Engelenburg, S. B. *et al.* Distribution of ESCRT machinery at HIV assembly sites reveals virus scaffolding of ESCRT subunits. *Science* **343**, 653-656, doi:10.1126/science.1247786 (2014).
182 Laine, R. F. *et al.* Structural analysis of herpes simplex virus by optical super-resolution imaging. *Nat Commun* **6**, 5980, doi:10.1038/ncomms6980 (2015).
183 Rincheval, V. *et al.* Functional organization of cytoplasmic inclusion bodies in cells infected by respiratory syncytial virus. *Nat Commun* **8**, 563, doi:10.1038/s41467-017-00655-9 (2017).
184 Fu, G. *et al.* In vivo structure of the E. coli FtsZ-ring revealed by photoactivated localization microscopy (PALM). *PLoS One* **5**, e12682, doi:10.1371/journal.pone.0012680 (2010).
185 Wang, W., Li, G. W., Chen, C., Xie, X. S. & Zhuang, X. Chromosome organization by a nucleoid-associated protein in live bacteria. *Science* **333**, 1445-1449, doi:10.1126/science.1204697 (2011).
186 Mostowy, S. *et al.* Entrapment of intracytosolic bacteria by septin cage-like structures. *Cell Host Microbe* **8**, 433-444, doi:10.1016/j.chom.2010.10.009 (2010).
187 Singh, M. K. & Kenney, L. J. Super-resolution imaging of bacterial pathogens and visualization of their secreted effectors. *FEMS Microbiol Rev*, doi:10.1093/femsre/fuaa050 (2020).
188 Williams, E. *et al.* The Image Data Resource: A Scalable Platform for Biological Image Data Access, Integration, and Dissemination. *bioRxiv* (2016).
189 Chen, S. Y., Heintzmann, R. & Cremer, C. Sample drift estimation method based on speckle patterns formed by backscattered laser light. *Biomed Opt Express* **10**, 6462-6475, doi:10.1364/BOE.10.006462 (2019).

190 Wang, Y. *et al.* Localization events-based sample drift correction for localization microscopy with redundant cross-correlation algorithm. *Opt. Express* **22**, 15982-15991, doi:10.1364/OE.22.015982 (2014).
191 McGorty, R., Kamiyama, D. & Huang, B. Active Microscope Stabilization in Three Dimensions Using Image Correlation. *Opt Nanoscopy* **2**, doi:10.1186/2192-2853-2-3 (2013).
192 Mlodzianoski, M. J. *et al.* Sample drift correction in 3D fluorescence photoactivation localization microscopy. *Opt. Express* **19**, 15009, doi:10.1364/OE.19.015009 (2011).
193 Lee, S. H. *et al.* Using fixed fiduciary markers for stage drift correction. *Opt Express* **20**, 12177-12183, doi:10.1364/oe.20.012177 (2012).
194 Grover, G., Mohrman, W. & Piestun, R. Real-time adaptive drift correction for super-resolution localization microscopy. *Opt. Express* **23**, 23887-23898, doi:10.1364/OE.23.023887 (2015).
195 Carter, A. R. *et al.* Stabilization of an optical microscope to 0.1 nm in three dimensions. *Appl. Opt.* **46**, 421-427, doi:10.1364/AO.46.000421 (2007).
196 Coelho, S. *et al.* Ultraprecise single-molecule localization microscopy enables in situ distance measurements in intact cells. *Science Advances* **6**, eaay8271, doi:10.1126/sciadv.aay8271 (2020).
197 Pertsinidis, A., Zhang, Y. & Chu, S. Subnanometre single-molecule localization, registration and distance measurements. *Nature* **466**, 647-651 (2010).
198 Culley, S. *et al.* Quantitative mapping and minimization of super-resolution optical imaging artifacts. *Nature Methods* **15**, 263-266, doi:10.1038/nmeth.4605 (2018).
199 Marsh, R. J. *et al.* Artifact-free high-density localization microscopy analysis. *Nat Methods* **15**, 689-692, doi:10.1038/s41592-018-0072-5 (2018).
200 Dertinger, T., Colyer, R., Iyer, G., Weiss, S. & Enderlein, J. Fast, background-free, 3D super-resolution optical fluctuation imaging (SOFI). *Proc Natl Acad Sci U S A* **106**, 22287-22292, doi:10.1073/pnas.0907866106 (2009).
201 Ram, S., Ward, E. S. & Ober, R. J. Beyond Rayleigh's criterion: A resolution measure with application to single-molecule microscopy. *Proceedings of the National Academy of Sciences* **103**, 4457-4462 (2006).
202 Gould, T. J., Verkhusha, V. V. & Hess, S. T. Imaging biological structures with fluorescence photoactivation localization microscopy. *Nat Protoc* **4**, 291-308, doi:10.1038/nprot.2008.246 (2009).
203 Cabriel, C., Bourg, N., Dupuis, G. & Lévêque-Fort, S. Aberration-accounting calibration for 3D single-molecule localization microscopy. *Opt. Lett.* **43**, 174-177, doi:10.1364/OL.43.000174 (2018).
204 Li, Y., Wu, Y.-L., Hoess, P., Mund, M. & Ries, J. Depth-dependent PSF calibration and aberration correction for 3D single-molecule localization. *Biomed. Opt. Express* **10**, 2708-2718, doi:10.1364/BOE.10.002708 (2019).
205 Engelhardt, J. *et al.* Molecular Orientation Affects Localization Accuracy in Superresolution Far-Field Fluorescence Microscopy. *Nano Lett.* **11**, 209-213, doi:10.1021/nl103472b (2011).
206 Cruz, C. A. V. *et al.* Quantitative nanoscale imaging of orientational order in biological filaments by polarized superresolution microscopy. *Proceedings of the National Academy of Sciences* **113**, E820-E828, doi:10.1073/pnas.1516811113 (2016).
207 Davis, J. L., Dong, B., Sun, C. & Zhang, H. F. Method to identify and minimize artifacts induced by fluorescent impurities in single-molecule localization microscopy. *J Biomed Opt* **23**, 1-14, doi:10.1117/1.JBO.23.10.106501 (2018).
208 Sigal, Y. M., Speer, C. M., Babcock, H. P. & Correspondence, X. Z. Mapping Synaptic Input Fields of Neurons with Super-Resolution Imaging In Brief. *Cell* **163**, 493-505, doi:10.1016/j.cell.2015.08.033 (2015).

209 German, C. L., Gudheti, M. V., Fleckenstein, A. E. & Jorgensen, E. M. Vol. 1663 153-162 (Humana Press Inc., 2017).
210 Xu, J. *et al.* Super-resolution imaging reveals the evolution of higher-order chromatin folding in early carcinogenesis. *Nat Commun* **11**, 1-17, doi:10.1038/s41467-020-15718-7 (2020).
211 Tobin, S. J. *et al.* Single molecule localization microscopy coupled with touch preparation for the quantification of trastuzumab-bound HER2. *Sci Rep* **8**, 15154, doi:10.1038/s41598-018-33225-0 (2018).
212 Archetti, A. *et al.* Waveguide-PAINT offers an open platform for large field-of-view super-resolution imaging. *Nat Commun* **10**, doi:10.1038/s41467-019-09247-1 (2019).
213 Douglass, K. M., Sieben, C., Archetti, A., Lambert, A. & Manley, S. Super-resolution imaging of multiple cells by optimized flat-field epi-illumination. *Nature Photonics* **10**, 705-708, doi:10.1038/nphoton.2016.200 (2016).
214 Stehr, F., Stein, J., Schueder, F., Schwille, P. & Jungmann, R. Flat-top TIRF illumination boosts DNA-PAINT imaging and quantification. *Nat Commun* **10**, doi:10.1038/s41467-019-09064-6 (2019).
215 Klevanski, M. *et al.* Automated highly multiplexed super-resolution imaging of protein nano-architecture in cells and tissues. *Nat Commun* **11**, 1-11, doi:10.1038/s41467-020-15362-1 (2020).
216 Jungmann, R. *et al.* Multiplexed 3D cellular super-resolution imaging with DNA-PAINT and Exchange-PAINT. *Nat Methods* **11**, 313-318, doi:10.1038/nmeth.2835 (2014).
217 Schueder, F. *et al.* Universal Super-Resolution Multiplexing by DNA Exchange. *Angew Chem Int Ed Engl* **56**, 4052-4055, doi:10.1002/anie.201611729 (2017).
218 Wade, O. K. *et al.* 124-Color Super-resolution Imaging by Engineering DNA-PAINT Blinking Kinetics. *Nano Lett* **19**, 2641-2646, doi:10.1021/acs.nanolett.9b00508 (2019).
219 Gómez-García, P. A., Garbacik, E. T., Otterstrom, J. J., Garcia-Parajo, M. F. & Lakadamyali, M. Excitation-multiplexed multicolor superresolution imaging with fm-STORM and fm-DNA-PAINT. *Proceedings of the National Academy of Sciences of the United States of America* **115**, 12991-12996, doi:10.1073/pnas.1804725115 (2018).
220 Zhuang, X. Spatially resolved single-cell genomics and transcriptomics by imaging. *Nat Methods* **18**, 18-22, doi:10.1038/s41592-020-01037-8 (2021).
221 Beghin, A. *et al.* Localization-based super-resolution imaging meets high-content screening. *Nature Methods* **14**, 1184-1190, doi:10.1038/nmeth.4486 (2017).
222 Almada, P. *et al.* Automating multimodal microscopy with NanoJ-Fluidics. *Nat Commun* **10**, 1-9, doi:10.1038/s41467-019-09231-9 (2019).
223 Huang, F. *et al.* Video-rate nanoscopy using sCMOS camera-specific single-molecule localization algorithms. *Nat Methods* **10**, 653-658, doi:10.1038/nmeth.2488 (2013).
224 Barentine, A. E. S. *et al.* 3D Multicolor Nanoscopy at 10,000 Cells a Day. *bioRxiv*, 606954-606954, doi:10.1101/606954 (2019).
225 Auer, A., Strauss, M. T., Schlichthaerle, T. & Jungmann, R. Fast, Background-Free DNA-PAINT Imaging Using FRET-Based Probes. *Nano Lett* **17**, 6428-6434, doi:10.1021/acs.nanolett.7b03425 (2017).
226 Lee, J., Park, S. & Hohng, S. Accelerated FRET-PAINT microscopy. *Mol Brain* **11**, 70, doi:10.1186/s13041-018-0414-3 (2018).
227 Lee, J., Park, S., Kang, W. & Hohng, S. Accelerated super-resolution imaging with FRET-PAINT. *Mol Brain* **10**, 63, doi:10.1186/s13041-017-0344-5 (2017).
228 Schueder, F. *et al.* An order of magnitude faster DNA-PAINT imaging by optimized sequence design and buffer conditions. *Nat Methods* **16**, 1101-1104, doi:10.1038/s41592-019-0584-7 (2019).
229 Filius, M. *et al.* High-Speed Super-Resolution Imaging Using Protein-Assisted DNA-PAINT. *Nano Lett* **20**, 2264-2270, doi:10.1021/acs.nanolett.9b04277 (2020).

230 Strauss, S. & Jungmann, R. Up to 100-fold speed-up and multiplexing in optimized DNA-PAINT. *Nat Methods*, doi:10.1038/s41592-020-0869-x (2020).
231 Diederich, B., Then, P., Jugler, A., Forster, R. & Heintzmann, R. cellSTORM-Cost-effective super-resolution on a cellphone using dSTORM. *PLoS One* **14**, e0209827, doi:10.1371/journal.pone.0209827 (2019).
232 Ma, H., Fu, R., Xu, J. & Liu, Y. A simple and cost-effective setup for super-resolution localization microscopy. *Sci Rep* **7**, 1542, doi:10.1038/s41598-017-01606-6 (2017).
233 Auer, A. *et al.* Nanometer-scale Multiplexed Super-Resolution Imaging with an Economic 3D-DNA-PAINT Microscope. *Chemphyschem* **19**, 3024-3034, doi:10.1002/cphc.201800630 (2018).
234 Cella Zanacchi, F. *et al.* Live-cell 3D super-resolution imaging in thick biological samples. *Nature Methods* **8**, 1047-1050, doi:10.1038/nmeth.1744 (2011).
235 Huisken, J., Swoger, J., Del Bene, F., Wittbrodt, J. & Stelzer, E. H. Optical sectioning deep inside live embryos by selective plane illumination microscopy. *Science* **305**, 1007-1009, doi:10.1126/science.1100035 (2004).
236 Waldchen, F. *et al.* Whole-cell imaging of plasma membrane receptors by 3D lattice light-sheet dSTORM. *Nat Commun* **11**, 887, doi:10.1038/s41467-020-14731-0 (2020).
237 Mlodzianoski, M. J. *et al.* Active PSF shaping and adaptive optics enable volumetric localization microscopy through brain sections. *Nat Methods* **15**, 583-586, doi:10.1038/s41592-018-0053-8 (2018).
238 Sochacki, K. A., Shtengel, G., van Engelenburg, S. B., Hess, H. F. & Taraska, J. W. Correlative super-resolution fluorescence and metal-replica transmission electron microscopy. *Nat Methods* **11**, 305-308, doi:10.1038/nmeth.2816 (2014).
239 Sochacki, K. A., Dickey, A. M., Strub, M. P. & Taraska, J. W. Endocytic proteins are partitioned at the edge of the clathrin lattice in mammalian cells. *Nat Cell Biol* **19**, 352-361, doi:10.1038/ncb3498 (2017).
240 Vassilopoulos, S., Gibaud, S., Jimenez, A., Caillol, G. & Leterrier, C. Ultrastructure of the axonal periodic scaffold reveals a braid-like organization of actin rings. *Nat Commun* **10**, 1-13, doi:10.1038/s41467-019-13835-6 (2019).
241 Dahlberg, P. D. *et al.* Cryogenic single-molecule fluorescence annotations for electron tomography reveal in situ organization of key proteins in Caulobacter. *Proc Natl Acad Sci U S A* **117**, 13937-13944, doi:10.1073/pnas.2001849117 (2020).
242 Hoffman, D. P. *et al.* Correlative three-dimensional super-resolution and block-face electron microscopy of whole vitreously frozen cells. *Science* **367**, doi:10.1126/science.aaz5357 (2020).
243 Xu, K., Babcock, H. P. & Zhuang, X. Dual-objective STORM reveals three-dimensional filament organization in the actin cytoskeleton. *Nat Methods* **9**, 185-188, doi:10.1038/nmeth.1841 (2012).
244 Shtengel, G. *et al.* Interferometric fluorescent super-resolution microscopy resolves 3D cellular ultrastructure. *Proc Natl Acad Sci U S A* **106**, 3125-3130, doi:10.1073/pnas.0813131106 (2009).
245 Huang, F. *et al.* Ultra-High Resolution 3D Imaging of Whole Cells. *Cell* **166**, 1028-1040, doi:10.1016/j.cell.2016.06.016 (2016).
246 Balzarotti, F. *et al.* Nanometer resolution imaging and tracking of fluorescent molecules with minimal photon fluxes. *Science* **355**, 606-612, doi:10.1126/science.aak9913 (2017).
247 Cnossen, J. *et al.* Localization microscopy at doubled precision with patterned illumination. *Nat Methods* **17**, 59-63, doi:10.1038/s41592-019-0657-7 (2020).
248 Gu, L. *et al.* Molecular resolution imaging by repetitive optical selective exposure. *Nat Methods* **16**, 1114-1118, doi:10.1038/s41592-019-0544-2 (2019).
249 Gwosch, K. C. *et al.* MINFLUX nanoscopy delivers 3D multicolor nanometer resolution in cells. *Nat Methods* **17**, 217-224, doi:10.1038/s41592-019-0688-0 (2020).

250 Chen, F., Tillberg, P. W. & Boyden, E. S. Expansion microscopy. *Science* **347**, 543-548, doi:10.1126/science.1260088 (2015).
251 Chang, J. B. *et al.* Iterative expansion microscopy. *Nat Methods* **14**, 593-599, doi:10.1038/nmeth.4261 (2017).
252 Tillberg, P. W. *et al.* Protein-retention expansion microscopy of cells and tissues labeled using standard fluorescent proteins and antibodies. *Nat Biotechnol* **34**, 987-992, doi:10.1038/nbt.3625 (2016).
253 Wen, G. *et al.* Evaluation of Direct Grafting Strategies via Trivalent Anchoring for Enabling Lipid Membrane and Cytoskeleton Staining in Expansion Microscopy. *ACS Nano*, doi:10.1021/acsnano.9b09259 (2020).
254 Shi, X. *et al.* Label-retention expansion microscopy. *bioRxiv*, 687954-687954, doi:10.1101/687954 (2019).
255 Zwettler, F. U. *et al.* Molecular resolution imaging by post-labeling expansion single-molecule localization microscopy (Ex-SMLM). *bioRxiv*, 2020.2003.2012.988923, doi:10.1101/2020.03.12.988923 (2020).
256 LeCun, Y., Bengio, Y. & Hinton, G. Deep learning. *Nature* **521**, 436-444, doi:10.1038/nature14539 (2015).
257 Mockl, L., Roy, A. R. & Moerner, W. E. Deep learning in single-molecule microscopy: fundamentals, caveats, and recent developments [Invited]. *Biomed Opt Express* **11**, 1633-1661, doi:10.1364/BOE.386361 (2020).
258 Nehme, E. *et al.* DeepSTORM3D: dense 3D localization microscopy and PSF design by deep learning. *Nat Methods* **17**, 734-740, doi:10.1038/s41592-020-0853-5 (2020).
259 Ouyang, W., Aristov, A., Lelek, M., Hao, X. & Zimmer, C. Deep learning massively accelerates super-resolution localization microscopy. *Nature Biotechnology* **36**, 460-468, doi:10.1038/nbt.4106 (2018).
260 Weigert, M. *et al.* Content-aware image restoration: pushing the limits of fluorescence microscopy. *Nature Methods* **15**, 1090, doi:10.1038/s41592-018-0216-7 (2018).
261 Falk, T. *et al.* U-Net: deep learning for cell counting, detection, and morphometry. *Nat Methods* **16**, 67-70, doi:10.1038/s41592-018-0261-2 (2019).
262 Haberl, M. G. *et al.* CDeep3M-Plug-and-Play cloud-based deep learning for image segmentation. *Nat Methods* **15**, 677-680, doi:10.1038/s41592-018-0106-z (2018).
263 Belthangady, C. & Royer, L. A. Applications, promises, and pitfalls of deep learning for fluorescence image reconstruction. *Nat Methods* **16**, 1215-1225, doi:10.1038/s41592-019-0458-z (2019).
264 Dempsey, G. T., Vaughan, J. C., Chen, K. H., Bates, M. & Zhuang, X. Evaluation of fluorophores for optimal performance in localization-based super-resolution imaging. *Nat Methods* **8**, 1027-1036, doi:10.1038/nmeth.1768 (2011).
265 Jradi, F. M. & Lavis, L. D. Chemistry of Photosensitive Fluorophores for Single-Molecule Localization Microscopy. *ACS Chem Biol* **14**, 1077-1090, doi:10.1021/acschembio.9b00197 (2019).
266 Li, Y. *et al.* Real-time 3D single-molecule localization using experimental point spread functions. *Nature Methods*, doi:10.1038/nmeth.4661 (2018).
267 Ries, J. SMAP: a modular super-resolution microscopy analysis platform for SMLM data. *Nat Methods* **17**, 870-872, doi:10.1038/s41592-020-0938-1 (2020).
268 Jimenez, A., Friedl, K. & Leterrier, C. About samples, giving examples: Optimized Single Molecule Localization Microscopy. *Methods* **174**, 100-114, doi:10.1016/j.ymeth.2019.05.008 (2020).
269 Manley, S., Gillette, J. M. & Lippincott-Schwartz, J. Single-particle tracking photoactivated localization microscopy for mapping single-molecule dynamics. *Methods Enzymol* **475**, 109-120, doi:10.1016/S0076-6879(10)75005-9 (2010).

270 Kaplan, C. & Ewers, H. Optimized sample preparation for single-molecule localization-based superresolution microscopy in yeast. *Nat Protoc* **10**, 1007-1021, doi:10.1038/nprot.2015.060 (2015).
271 Nieuwenhuizen, R. P. J. *et al.* Measuring image resolution in optical nanoscopy. *Nature methods* **10**, 557-562, doi:10.1038/nmeth.2448 (2013).
272 Descloux, A., Grussmayer, K. S. & Radenovic, A. Parameter-free image resolution estimation based on decorrelation analysis. *Nat Methods* **16**, 918-924, doi:10.1038/s41592-019-0515-7 (2019).
273 Bates, M., Huang, B., Dempsey, G. T. & Zhuang, X. Multicolor Super-Resolution Imaging with Photo-Switchable Fluorescent Probes. *Science*, 1146598v1146591 (2007).
274 Flottmann, B. *et al.* Correlative light microscopy for high-content screening. *Biotechniques* **55**, 243-252, doi:10.2144/000114099 (2013).
275 Yan, R., Moon, S., Kenny, S. J. & Xu, K. Spectrally Resolved and Functional Super-resolution Microscopy via Ultrahigh-Throughput Single-Molecule Spectroscopy. *Acc Chem Res* **51**, 697-705, doi:10.1021/acs.accounts.7b00545 (2018).
276 Testa, I. *et al.* Multicolor fluorescence nanoscopy in fixed and living cells by exciting conventional fluorophores with a single wavelength. *Biophys J* **99**, 2686-2694, doi:10.1016/j.bpj.2010.08.012 (2010).
277 Dong, B. *et al.* Super-resolution spectroscopic microscopy via photon localization. *Nat Commun* **7**, 12290, doi:10.1038/ncomms12290 (2016).
278 Muranyi, W., Malkusch, S., Muller, B., Heilemann, M. & Krausslich, H. G. Super-resolution microscopy reveals specific recruitment of HIV-1 envelope proteins to viral assembly sites dependent on the envelope C-terminal tail. *PLoS Pathog* **9**, e1003198, doi:10.1371/journal.ppat.1003198 (2013).
279 Pavani, S. R. P. *et al.* Three-dimensional, single-molecule fluorescence imaging beyond the diffraction limit by using a double-helix point spread function. *Proceedings of the National Academy of Sciences of the United States of America* **106**, 2995-2999 (2009).
280 Juette, M. F. *et al.* Three-dimensional sub-100 nm resolution fluorescence microscopy of thick samples. *Nature Methods* **5**, 527-529 (2008).
281 Abrahamsson, S. *et al.* Fast multicolor 3D imaging using aberration-corrected multifocus microscopy. *Nature Methods* **10**, 60-63, doi:10.1038/NMETH.2277 (2013).
282 Hajj, B., Beheiry, M. E., Izeddin, I., Darzacq, X. & Dahan, M. Accessing the third dimension in localization-based super-resolution microscopy. *Physical Chemistry Chemical Physics* **16**, 16340-16348, doi:10.1039/C4CP01380H (2014).
283 Shechtman, Y., Sahl, S. J., Backer, A. S. & Moerner, W. E. Optimal point spread function design for 3D imaging. *Physical Review Letters* **113**, doi:10.1103/PhysRevLett.113.133902 (2014).
284 Ram, S., Prabhat, P., Ward, E. S. & Ober, R. J. Improved single particle localization accuracy with dual objective multifocal plane microscopy. *Opt Express* **17**, 6881-6898, doi:10.1364/oe.17.006881 (2009).